View metadata, citation and similar papers at core.ac.uk

brought to you by CORE

provided by NASA Technical Reports Server

NASA Technical Memorandum 86838

NASA-TM-86838 19880014366

# PAN AIR Analysis of the NASA/MCAIR 279-3: An Advanced Supersonic V/STOL Fighter/Attack Aircraft

M.D. Madson and L.L. Erickson

LIBRARY COPY

MAY 19 1986

LANGLEY RESEARCH CENTER
LIBRARY, NASA
HAMPTON, VIRGINIA

April 1986

~~LIMITED DISTRIBUTION DOCUMENT~~

~~Because of its significant technological potential, this information, which has been developed under a U.S. Government program, is being given a limited distribution whereby advanced access is provided for use by domestic interests. This legend shall be marked on any reproduction of this information in whole or in part.~~

Date for general release April 1988

National Aeronautics and Space Administration

NF00079

NASA Technical Memorandum 86838

3 1176 01327 7042

# PAN AIR Analysis of the NASA/MCAIR 279-3: An Advanced Supersonic V/STOL Fighter/Attack Aircraft

M. D. Madson,
L. L. Erickson, Ames Research Center, Moffett Field, California

April 1986

National Aeronautics and
Space Administration

**Ames Research Center**
Moffett Field, California 94035

This Page Intentionally Left Blank

## SYMBOLS

$a,b,c,d,e$ = coefficients in general boundary condition equation

$\bar{c}$ = mean aerodynamic chord

$C_L$ = lift coefficient

$C_{L_\alpha}$ = lift curve slope, per degree

$C_M$ = pitching moment coefficient, $0.08\ \bar{c}$

$M_\infty$ = free-stream Mach number

$\hat{n}$ = surface unit normal vector

$s$ = sign $(1 - M_\infty^2)$

$\vec{t}$ = surface tangent vector

$\vec{U}_\infty$ = uniform onset flow

$\vec{v}$ = perturbation velocity

$\vec{W}$ = total mass-flux

$\vec{w}$ = perturbation mass-flux

$x,y,z$ = Cartesian coordinates

$\alpha$ = angle of attack, degrees

$\beta$ = $\sqrt{|1 - M_\infty^2|}$

$\mu$ = doublet strength

$\phi$ = perturbation potential

$\bar{\Phi}$ = total mass-flux potential

$\vec{\Psi}$ = $(x/s\beta^2, y, z)$

Subscripts

EXT = exterior geometry (i.e., wetted by real flow)

INT = interior geometry (i.e., not wetted by real flow)

## SUMMARY

PAN AIR is a computer program for predicting subsonic or supersonic linear potential flow about arbitrary configurations. The program was applied to a highly complex single-engine-cruise V/STOL fighter/attack aircraft. Complexities include a close-coupled canard/wing, large inlets, and four exhaust nozzles mounted directly under the wing and against the fuselage. Modeling uncertainties involving canard wake location and flow-through approximation through the inlet and the exhaust nozzles were investigated. The recently added streamline capability of the program was utilized to evaluate visually the predicted flow over the model. PAN AIR results for Mach numbers of 0.6, 0.9, and 1.2 at angles of attack of 0, 5, and 10° were compared with data obtained in the Ames 11- by 11-Foot Transonic Wind Tunnel, at a Reynolds number of $3.69 \times 10^6$ based on $\bar{c}$.


## INTRODUCTION

A jointly sponsored NASA Ames and Navy program was initiated in 1980 to develop aerodynamic technology for post-1990, single-cruise-engine vertical/short takeoff, landing (V/STOL) fighter/attack aircraft. One of the configurations that arose from this program was the McDonnell Aircraft Company (MCAIR) 279-3 (from here on referred to as the "279"). The wind tunnel force model of the 279 is shown in figure 1.

One of the goals of the project was to determine how well the aerodynamics of complex configurations could be analytically predicted. Although much progress has been made in the field of computational fluid dynamics in recent years, only linear panel codes are currently able to deal with the geometric complexity of configurations such as the 279. PAN AIR (refs. 1-8) is one of the few panel codes that treats both subsonic and supersonic flow. Except for the case of incompressible flow ($M_\infty = 0$), the linear theory upon which PAN AIR is based, namely the Prandtl-Glauert equation, assumes that local flow velocities do not differ greatly from the free-stream velocity. Consequently the theory is particularly valid for very slender configurations. This is especially true at supersonic free-stream Mach numbers. In contrast, the geometry of the 279 is relatively non-slender. The present investigation was undertaken to determine what degree of success could be achieved by applying PAN AIR to the nonslender geometry of the 279.

Several PAN AIR models were examined to determine the effect of canard wake position and nozzle-exit flow modeling on the predicted aerodynamics. The recent addition of the program's streamline capability was used to visualize the resulting

flow about the model. PAN AIR force and moment results for Mach numbers of 0.6, 0.9, and 1.2 for the baseline canard/wing configuration as well as a canard-off configuration were compared to data obtained in the NASA Ames 11- by 11-Foot Transonic Wind Tunnel, at a Reynolds number of $3.69 \times 10^6$ based on $\bar{c}$.

## PAN AIR MODEL DEVELOPMENT

### Description of the Model

The 279 configuration employs a close-coupled canard/wing, has large inlets for a high bypass ratio engine, and has a maximum design Mach number of 2.0. The configuration also has four deflecting exhaust nozzles, for thrust-vectoring capability similar to that of the Harrier aircraft. The PAN AIR definition of the 279 was modeled for the case of zero nozzle deflection only.

Cross-sectional information for the model was obtained from MCAIR using the Initial Graphic Exchange Specification (IGES) format as the means for transferring the information between computer-aided design/computer-aided manufacturing (CAD/CAM) systems. The PAN AIR model of the 279 was constructed on a Calma CAD/CAM system. For configurations symmetric about the x-z plane, PAN AIR allows the user to input only one side of the geometry. The program was told to account for the other side of the model in its calculations. The PAN AIR model (right side only) consists of 990 source/doublet panels, 184 doublet wake panels for the subsonic model, and 243 doublet wake panels for the supersonic model. Figure 2 shows the right-hand side PAN AIR definition of the model, along with the symmetric left-hand side. Except for the inlet and nozzle exit-plane networks (to be described in a later section), the impermeable surface geometry was modeled using PAN AIR's class 1 boundary conditions (ref. 6, appendix B.3.1). This corresponds to:

$$(\vec{W} \cdot \hat{n})_{EXT} = 0$$

$$\phi_{INT} = 0$$

Note that the aft tips of the outriggers and the fuselage are truncated in the PAN AIR definition. These truncated tips, together with base networks having constant total potential boundary conditions on the downstream side and wake networks (not shown), were used to simulate flow separation from the aft end of the fuselage and outrigger surfaces. A more detailed explanation of this flow separation model is presented in figure 18(d) of reference 3.

The wind tunnel model of the 279 has a sting shroud attached to the lower aft portion of the fuselage (fig. 1(b)). The PAN AIR model of the 279 did not include the sting shroud. Consequently, aerodynamic effects caused by the presence of the shroud on the wind tunnel model are not represented in the computations.

## PAN AIR Canard Wake Position

PAN AIR does not solve for the shape and position of a wake from a lifting surface. It is up to the user to define the positions and shapes of the wakes for a particular geometry. For close-coupled canard/wing configurations such as the 279, it has been shown (ref. 4) that the position of the canard wake relative to the wing can have a substantial effect on the total computed lift of the aircraft as the angle of attack increases. Figure 3 shows the root sections of the canard and the wing at zero angle of attack, with wakes defined in the chord plane. The canard wake passes near to the upper surface of the wing. Since the wing has a 9° anhedral, the vertical distance between the canard wake and the wing increases in the outboard direction (fig. 1(a)). If this canard wake location remains fixed through a wide range of angles of attack, the wing circulation distribution begins to be seriously affected. Figures 4(a) and 4(b) show PAN AIR lift and pitching moment results at $M_\infty = 0.6$ for two cases. The first case defines a canard wake location that remains unchanged with angle of attack, i.e., fixed relative to the model. The second case defines a canard wake location which is aligned with, i.e., parallel to, the free stream at each angle of attack. For simplicity, wakes from the wing and the outrigger were not aligned for either of the two canard wake cases. Reference 4 shows that this simplification does not affect the solution when the wakes are not passing over (or under) another lifting surface.

Figure 4(a) shows the $C_{L_\alpha}$ predicted by PAN AIR for the two wake models. The aligned canard wake case yields a 5% increase in $C_{L_\alpha}$ over the fixed canard wake case. This increase brings the PAN AIR predicted value of $C_{L_\alpha}$ to within 5% of the $C_{L_\alpha}$ obtained from the experimental data. The effect of the canard wake position on the predicted pitching moment is shown in figure 4(b). For the given $C_L$ range, the wind tunnel results are nonlinear. The linear range is restricted to $C_L$'s between 0.15 and 0.30. For this linear region, $dC_M/dC_L$ is 0.089. For the fixed-canard wake case, $dC_M/dC_L$ is 0.10. For the aligned-canard wake case, $dC_M/dC_L$ is 0.095. Figures 4(a) and 4(b) show that the aligned canard wake case yields results that compare more favorably with experimental data.

Figure 4(c) shows the PAN AIR results for the spanwise doublet distribution (a measure of the spanwise lift distribution) along the canard and wing wakes for the two canard wake cases. The reference value of the doublet strength, $\mu_{ref}$, was chosen to be the doublet strength value at the root of the canard for the aligned canard wake case. Figure 4(c) shows that the position of the canard wake does not significantly affect the lift distribution along the canard. It does, however, have an important effect on the predicted lift distribution along the wing. Moving the canard wake from the fixed position to the aligned position causes two major changes in the flow over the wing. The dominant effect is an increase in wing lift inboard of the canard tip station. This is due to the diminished canard wake downwash field, raising the effective angle of attack of the inboard wing section. The secondary effect is a loss in wing lift outboard of the canard tip station. This loss in lift is due to diminished spanwise velocity imparted on the upper surface of the wing by the canard wake, which is due to the increased distance between the

canard wake and the wing. The net effect of these changes in the local flow field is the increase in predicted total lift shown in figure 4(a).

When the canard wake is defined in a manner such as that shown in figure 3, the inboard edge of the wake abuts empty space. This situation occurs because the fuselage geometry aft of the canard root slopes below the chord line in which the canard wake is defined. To prevent the doublet strength at the inboard edge of the canard wake from being set to zero because of this empty space abutment, a constant doublet strength wake network (in PAN AIR, a wake type DW2) is defined which connects the inboard edge of the canard wake and the outboard edge of the fuselage geometry aft of the canard root. This causes the doublet strength at the inboard edge of the canard wake to be conserved, rather than being set to zero, as shown in figure 4(c). More will be said about properly defining a wake type DW2 network in a later section.

## Modeling Flow-Through Ducts

The wind tunnel model of the 279 is a flow-through model. The internal nacelle definition was not modeled for PAN AIR because of the complexity of the internal geometry and the large number of additional panels which would be required to adequately represent the geometry. Consequently, a simpler, less costly approach was sought in which the flow-through behavior was approximated by controlling the flow conditions at the inlet and exit planes.

The inlet flow was controlled with boundary conditions applied to a set of panels at the inlet face (fig. 2(a)). For subsonic flow, the boundary conditions imposed at a source/doublet panel separating two flow domains must describe the flow on both sides of the panel. The same condition is true for supersonic flow unless the panel is inclined more steeply to the free stream than is the Mach cone, in which case it becomes, in PAN AIR nomenclature, a "super-inclined" panel. A super-inclined panel must not have boundary conditions that specify flow on the upstream side of the panel (ref. 6, appendix A.3.3.2), so both boundary conditions must be used to specify flow properties on the downstream side of the panel. The inlet network on the 279 model is super-inclined in supersonic flow. Thus, the subsonic and supersonic boundary conditions on the inlet network by necessity have to be different. These boundary conditions are described in detail in the sections on supersonic and subsonic flow-through modeling.

Some of the exit flow models investigated also used a network of panels at the nozzle exit planes (fig. 2(b)). These so-called "base" networks are super-inclined in supersonic flow. Consequently, the boundary conditions again depend on whether the flow is subsonic or supersonic. The nozzle exit boundary conditions are discussed in more detail in the next sections.

Four nozzle exit flow models were studied. These models (table 1) are combinations of using/not-using base networks and wakes. All four models were studied for the supersonic case, but only the models with base networks at the nozzle exit planes (Models 3 and 4) were studied for the subsonic case.

The models without base networks were not studied for the subsonic case because in subsonic flow, unlike supersonic flow, the absence of base networks allows downstream geometry to influence the flow in the interior volume of the PAN AIR model. This influence could cause the interior potential to no longer be uniformly zero; this is in conflict with the class 1 boundary condition assumption. The presence of base networks at the nozzle exit-planes, with the proper boundary conditions, prevents the exterior flow from influencing the interior potential.

Model 1, which is without nozzle wakes and base networks at the nozzle exit-planes, would not normally be considered a good model since the free edges at the aft end of the nozzles cause the doublet strength to go to zero at those edges. This causes large doublet strength gradients and unrealistically large local velocities. A PAN AIR option is available to suppress doublet matching at specified network edges, thus preventing the doublet strength from being forced to zero at those edges. This option applied to Model 1 makes this model appealing because of its simplicity. Unfortunately, the complexity of the geometry in the nozzle region caused an error in PAN AIR when this option was applied. Thus, results for Model 1 were obtained without the doublet matching being suppressed and are, as will be shown, predictably poor.

A discussion of the boundary conditions applied to the inlet and exit planes for supersonic and subsonic flow is presented below. The results for the four models are also presented, along with conclusions as to which models gave the best results for both subsonic and supersonic flow.

Supersonic Flow-Through Modeling- The problem of knowing what constitutes a well-posed or ill-posed boundary value problem for supersonic flow is not as well understood as it is for subsonic flow (ref. 6, appendix A). For example, the claim is made in section A.3.3.2 of reference 6 that permissible choices for two independent boundary conditions on the downstream side of a superinclined panel can be formed from the following equation:

$$a(\vec{w} \cdot \hat{n}) + c\phi + d\,\frac{\partial \phi}{\partial t} + e\,\frac{\partial \phi}{\partial n} = b$$

This is evidently not true since, for $M_\infty = 1.2$, the boundary conditions

$$\frac{\partial \phi}{\partial t} = \vec{v} \cdot \vec{t} = 0$$

$$\frac{\partial \phi}{\partial n} = \vec{v} \cdot \hat{n} = 0$$

imposed on the downstream side of the super-inclined nacelle exit plane networks for Model 3 (no nozzle wakes) caused an error in PAN AIR during the decomposition of the aerodynamic influence coefficient (AIC) matrix. This error apparently occurred because the AIC matrix was singular, reflecting an ill-posed boundary value problem.

Experience has shown (ref. 7, case 3) that the boundary conditions

$$\vec{w} \cdot \hat{n} = 0$$

$$\phi = 0$$

applied to the downstream side of a super-inclined panel constitutes a well-posed boundary value problem. These two boundary conditions were used for both the inlet and the exit plane networks. Physically, this corresponds to having no perturbation velocity at the downstream side of the network, with no effect being produced on the upstream side. Thus, the flow into the inlet should not be affected by the presence of the inlet plane network, and the flow out of the exit-plane networks should be the free-stream velocity since, with class 1 boundary conditions, the perturbation potential is zero in the interior volume of the PAN AIR model. At $\alpha = 0$ and $M_\infty = 1.2$, the PAN AIR computed inlet flow velocities at the panel centers varied from 75% of free stream at the top panel, to 93% at the bottom panel. Although no experimental results are available for comparison, these values are considered reasonable for the given inlet geometry. Computed values of the velocity flowing out of the exit plane networks confirmed that it is essentially free stream for both Models 3 and 4.

Lift and pitching moment results for the four models are shown in figure 5. Results based on both second-order and isentropic pressure formulas are given. The best lift results were obtained by the two models with nozzle wakes (Models 2 and 4). The results for these models were essentially identical. For Models 2 and 4, PAN AIR predicts a value of $C_{L_\alpha}$ with the second-order formula that is nearly parallel to the experimental curve. The value of $C_{L_\alpha}$ using the isentropic formula is 12% lower than the experimental curve. The lift predictions for the two models without nozzle wakes (Models 1 and 3) were much poorer in comparison, as shown in figure 5(a).

Figure 5(b) shows that the models without nozzle wakes also yielded poor pitching moment results. The models with nozzle wakes were not as clearly superior in predicting the pitching moment as they were in predicting the lift. The best comparison with the experimental data was the isentropic prediction for the models with nozzle wakes. The second-order prediction for these models compared poorly with the experimental data.

The results presented in figure 5 show that nozzle wakes are necessary in order for this particular configuration to generate useful supersonic aerodynamic data from PAN AIR. The presence of base networks at the nozzle exit-planes is desirable since flow quantities can then be calculated at the exit-planes, rather than being

assumed. For this reason, Model 4 was used to obtain all supersonic PAN AIR data presented in this paper, even though Model 2 yielded nearly identical results.

Subsonic Flow-Through Modeling- For the subsonic model without nozzle wakes (Model 3), the boundary conditions on the inlet network and the nozzle exit-plane networks were: (1) perturbation potential ($\phi$) on the interior side equal to zero, and (2) perturbation mass-flux across the network $[(\vec{w}_{EXT} - \vec{w}_{INT}) \cdot \hat{n}]$ equal to zero. These boundary conditions, in conjunction with the zero perturbation potential on the interior sides of the aircraft paneling, will cause approximately free-stream flow to enter the inlet network and exit from the nozzle exit-plane networks. The tangential velocities across the exit-plane networks were less than 10% of the free-stream velocity for the 0 to 10° angle-of-attack range that was investigated with PAN AIR.

For the model with nozzle wakes (Model 4), the boundary conditions on the nozzle exit-plane networks were: (1) perturbation potential ($\phi$) on the interior side equal to zero, and (2) doublet strength ($\mu$) equal to $-\vec{U}_\infty \cdot \vec{\Psi}$. This set of boundary conditions sets the total mass-flux potential ($\bar{\Phi}$) equal to zero on the downstream side of the networks. The inlet network boundary conditions remained the same as for Model 3. This set of boundary conditions as applied to the inlet network, and the boundary conditions and wakes as applied to the exit-plane base networks, is common for subsonic PAN AIR analysis.

The PAN AIR results for these models and their comparison with experimental data are shown in figure 6. Whereas in the supersonic case, the presence of nozzle wakes was required for any reasonable results to be obtained from PAN AIR, the opposite was found for the subsonic case. The addition of nozzle wakes to the geometry adversely affected subsonic PAN AIR results for both lift and pitching moment. This anomaly will be addressed in future numerical studies and wind tunnel experiments. Based on these results, the model without nozzle wakes (Model 3) was used to obtain all subsequent subsonic PAN AIR data.

In figure 7, the subsonic and supersonic nozzle exit-plane models used to obtain the PAN AIR data for this report are summarized. Figure 7(a) shows a schematic of the nozzle area, with the boundary conditions used on the nozzle exit-plane networks, for the model used to obtain subsonic PAN AIR results (Model 3). The boundary conditions on the nozzle exit-plane networks and nozzle wake information for the supersonic model (Model 4) are given on the nozzle area schematic in figure 7(b). The nozzle wakes defined for the supersonic model are shown in figure 8.

## PAN AIR Streamline Analysis

As a means of visualizing the flow over the 279 as predicted by PAN AIR, the recently added streamline capability of the program was utilized. As was mentioned in the previous section, an approximation of flow-through conditions at the nozzle exits without the use of nozzle wakes produced the best results for subsonic flow.

To verify that the flow was behaving reasonably aft of the nozzles with the given boundary conditions at the nozzle exit-planes (Fig. 7b), PAN AIR streamlines were generated for $\alpha = 5°$ and $M_\infty = 0.6$. The streamlines were given starting points around the outside perimeter of the inlet area, and around the exhaust nozzles. The resultant PAN AIR predicted streamlines are shown in figure 9.

This figure shows that the boundary conditions on the nozzle exit-planes cause the flow to move smoothly downstream, without the severe changes of direction that might appear with a poorly modeled nozzle exit-plane. For example, if the exit-plane networks had been modeled as impermeable surfaces, the potential flow solution would cause streamlines to wrap around the end of the nozzles, to move tangentially across the exit-planes, and then change direction again to follow the fuselage contour downstream. Figure 9 demonstrates the effectiveness of the streamline capability of PAN AIR as both a diagnostic tool, and as an aid in understanding the aerodynamics of complex aircraft geometries.

## Defining a PAN AIR Wake Type DW2 Network

When defining wakes for a PAN AIR model, two types of wake models are available. The first, referred to as wake type DW1, allows the doublet strength to vary spanwise, thus producing shed vorticity. The doublet strength remains constant in the streamwise direction. Control points lie along the edge of the wake that abuts the trailing edge of the lifting surface. These control points exist at panel edge center points and at network corner points. Since the outboard edge of the wake abuts empty space, the doublet strength is zero at this edge. A problem in defining the wake geometry for a model can occur at the intersection of the wing with the fuselage. Typically, the fuselage tapers off behind the trailing edge of the wing. The inboard edge of the wing wake is generally defined to have a constant spanwise location. This causes a gap to open up between the fuselage and the inboard edge of the wing wake. If this gap is not closed, the doublet strength at the inboard edge of the wing wake will also go to zero since it abuts empty space. This will cause a spurious loss of circulation at the root section of the wing. To solve this problem, the program allows the user to define a wake type DW2 to fill the gap. Figure 10 shows a schematic of this type of modeling. A type DW2 wake has one control point which exists at the origin of the wake network, and the doublet strength is constant throughout the network. By filling the gap between the fuselage and the inboard edge of the wing wake, the doublet strength at the inboard edge of the wing wake is conserved, rather than being set to zero.

The user must exercise caution when utilizing wake type DW2 networks. Since only one control point exists, it must be located at the inboard edge of the wing wake (point A in fig. 10), and not at the aft end of the fuselage (point B in fig. 10). The doublet strength at the aft end of the fuselage could be, and usually is, vastly different from the doublet strength at the inboard edge of the wing wake. This difference in doublet strengths can cause substantial differences in both lift and moment predictions. The original wake definition for the 279 erroneously defined the wake type DW2 between the fuselage and the inboard edge of

the wing wake so that the origin of the wake occurred at the aft end of the fuselage. When this error was found, it was corrected, and different results were predicted. It is not immediately obvious from the lift curves predicted with the two different origins which is the better model. It is seen in figure 11(a) that the lift curve shifted to the right when moving the origin to the proper location. This shift caused an improved zero-lift angle-of-attack prediction, but caused the lift to become underpredicted at the nonzero angles of attack. The pitching moment prediction was much clearer in showing the importance of the proper origin location for a wake type DW2 network. Figure 11(b) shows that moving the origin to the proper location caused the pitching moment curve to shift substantially to the left. This shift greatly improved PAN AIR's agreement with experimental data.

The preceding sections have discussed the development of the PAN AIR models for subsonic and supersonic analysis. The following section compares the PAN AIR predictions for these models with data obtained in the Ames 11- by 11-Foot Transonic Wind Tunnel.

## COMPARISON WITH WIND TUNNEL DATA

Two configurations were defined for PAN AIR analysis and for comparison with experimental data. The canard/wing, or baseline, configuration was of primary interest. A canard-off configuration was also analyzed. Wind tunnel results for the canard-off configuration were obtained to determine the effect of the canard on the aircraft aerodynamics. The PAN AIR analysis of the canard-off configuration was done primarily to determine how accurately PAN AIR could predict the aerodynamics of a close-coupled wing/canard model relative to a wing-alone configuration. Although the effect of the canard and its deflection angle on the overall aerodynamics is an important study, this analysis is saved for future work beyond this paper.

Several observations were made about the results that were common for both the baseline and the canard-off cases. The lift-curve slope predicted by PAN AIR using the second-order pressure rule was always higher than that predicted using the isentropic rule. The second-order lift predictions also compared more favorably with experimental data. Subsonically, PAN AIR underpredicted the total lift for the nonzero angles of attack. For $M_\infty = 1.2$, the second-order lift-curve slope nearly paralleled that of the experimental data, and the total lift predicted by the second-order rule was higher than that obtained in the wind tunnel. Over-predicted lift is generally expected from inviscid analysis codes such as PAN AIR, unless the decambering effect of the boundary layer is represented. The presence of the canard caused a higher degree of nonlinearity in the predicted pitching moment from both PAN AIR and the wind tunnel when compared with the canard-off case.

Large discrepancies between second-order and isentropic results indicate that there are substantial regions on the PAN AIR model where the local flow velocities are not small when compared to the free-stream velocity, thus violating the small perturbation assumptions of the Prandtl-Glauert equation. It can be shown (ref. 9),

however, that the second-order pressure formula identically satisfies the momentum equation when written in terms of the linearized mass-flux vector. Consequently, results obtained with the second-order formula are often less in error than the isentropic formula.

A discussion of the results for the canard-off and baseline configurations is presented below. Results from the PAN AIR analysis are presented, along with wind tunnel data, and the predictions published by MCAIR (ref. 10).

## Canard-Off Results

For $M_\infty = 0.6$, PAN AIR results for both isentropic and second-order pressure rules compared very closely with experimental data. Lift and pitching-moment results for this Mach number are given in figure 12. The second-order prediction for $C_{L_\alpha}$ of 0.057 was just slightly lower than the 0.058 value obtained from the wind tunnel data. The isentropic prediction was approximately 5% lower than the experimental data. The MCAIR prediction for $C_{L_\alpha}$ was 10% higher than the wind tunnel curve. The pitching-moment curve predicted by MCAIR is nearly parallel to that of the experimental data, though slightly offset to the right. For angles of attack of 5° and 10°, PAN AIR results for both isentropic and second-order pressure rules lie nearly on top of the curve of the experimental data. For $\alpha = 0$, however, the pitching moment values predicted by PAN AIR are somewhat lower than are the wind tunnel data.

For Mach numbers in the transonic range, linear potential codes such as PAN AIR do not account for important nonlinear effects such as shocks. Sometimes these effects are fairly local, and reasonable lift and moment predictions can be obtained. In this case, results were obtained for $M_\infty = 0.9$ that were useful. Figure 13 presents the lift and pitching moment results obtained for this Mach number. Wind tunnel results became nonlinear at an angle of attack of approximately 5°. PAN AIR results for $C_{L_\alpha}$ using the isentropic and second-order pressure rules were lower than wind tunnel results by 18% and 6% respectively. The MCAIR prediction for $C_{L_\alpha}$ was approximately 3% higher than the experimental curve. Results for the pitching moment were also encouraging. The isentropic curve and the MCAIR prediction for $dC_M/dC_L$ were approximately 5% higher than the wind tunnel prediction. The second-order curve was approximately 12% higher than experimental results.

The maximum Mach number that PAN AIR could analyze for this particular model was 1.2. The bluntness of the model and the high density paneling of the round leading edge of the wing prohibited the program from analyzing a higher Mach number. Many of the surface panels on the model would become superinclined at a higher Mach number, and the results generated for those panels would be unpredictable and unreliable. The lift and pitching moment results obtained for $M_\infty = 1.2$ are shown in figure 14. The second-order PAN AIR prediction for $C_{L_\alpha}$ nearly parallels the experimental data. The isentropic $C_{L_\alpha}$ is 13% lower than

the wind tunnel curve. MCAIR predicts a $C_{L_\alpha}$ approximately 13% higher than the experimental data. The MCAIR pitching-moment curve lies directly on top of the wind tunnel curve until a $C_L$ of approximately 0.37, after which it drops off slightly. The isentropic prediction for $dC_M/dC_L$ is nearly parallel to the wind tunnel results, and is shifted slightly to the right. For angles of attack of 5° and 10°, second-order predictions for $C_M$ lie close to the wind tunnel data. For $\alpha = 0$, the predicted moment is somewhat lower than the value that was obtained in the wind tunnel.

## Baseline (Canard-On) Results

For $M_\infty = 0.6$, PAN AIR results for both isentropic and second-order pressure rules compared closely with experimental data, though not as closely as they did for the canard-off case. These lift and pitching moment results are presented in figure 15. The second-order prediction for $C_{L_\alpha}$ was 5% lower than that obtained from the wind tunnel. The isentropic prediction was approximately 10% lower than the experimental data. The MCAIR prediction for $C_{L_\alpha}$ was essentially parallel to the wind tunnel curve. The pitching moment data from the wind tunnel is nonlinear. The linear range is limited to $C_L$'s between 0.15 and 0.30. For this range, the MCAIR prediction of the pitching moment curve is parallel to the experimental data, but the curve is shifted substantially to the right of the experimental curve. PAN AIR results miss slightly on the prediction of $dC_M/dC_L$, but the predicted moment values compare more favorably with the experimental results than those predicted by MCAIR.

As was mentioned in the section which presented the canard-off data, results obtained for Mach numbers in the transonic range by linear potential codes such as PAN AIR cannot be expected to be consistently accurate. In this case, as in the canard-off case, results obtained for $M_\infty = 0.9$ were useful. Figure 16 presents the lift and pitching moment results obtained for this Mach number. Again, MCAIR predictions for lift and $C_{L_\alpha}$ compared well with wind tunnel data. PAN AIR's second-order prediction for $C_{L_\alpha}$ was approximately 8% low, and the isentropic prediction was approximately 8% low compared with experimental data. As in the $M_\infty = 0.6$ case, pitching moment results from the wind tunnel were nonlinear. Again, the linear range was limited to $C_L$'s between 0.15 and 0.30. For this range, both the MCAIR prediction and PAN AIR's isentropic prediction for $dC_M/dC_L$ are essentially parallel to the experimental curve. These curves are shifted to the right by a substantial distance, as was the pattern for $M_\infty = 0.6$.

The lift and pitching moment results obtained for $M_\infty = 1.2$ are presented in figure 17. The second-order PAN AIR prediction for $C_{L_\alpha}$ is parallel to the experimental data, as was the result for the canard-off case. The isentropic curve is 11% lower when it is compared to the wind tunnel curve. The MCAIR prediction for $C_{L_\alpha}$ was approximately 10% higher than that obtained from the experimental data. Pitching moment comparisons with wind tunnel results were poor for this

case. The second-order prediction and the MCAIR prediction were not close when their values for $dC_M/dC_L$ or their pitching moment predictions for any given lift coefficient were considered. Although the isentropic results were nonlinear, they did the best job of predicting $dC_M/dC_L$ and the individual pitching moment values.

## CONCLUSIONS

The results presented in this paper have demonstrated the ability of PAN AIR to effectively predict the aerodynamics of a complex aircraft geometry in subsonic or supersonic flow under cruise-type conditions.

For this close-coupled canard/wing configuration, the location of the canard wake relative to the free stream had a large impact on PAN AIR results. Defining a canard wake which is parallel to the free stream yielded results that compared much better with experimental data than did the case of a canard wake which remained in a fixed position relative to the geometry through an angle-of-attack range.

The wind tunnel model of the 279 is a flow-through model, the internal definition of which was not available for the PAN AIR model. Four models which approximated flow-through conditions at the nozzle exit-planes were evaluated. These models are combinations of using/not-using nozzle wakes and base networks at the nozzle exit-planes. The best supersonic results were obtained using a flow-through approximation model consisting of base networks at the nozzle exit-planes and wakes off the nozzles. The model which generated the best subsonic results consisted of base networks at the nozzle exit-planes with no wakes off the nozzles.

PAN AIR's streamline capability was utilized to evaluate visually the predicted flow in the vicinity of the nozzle exit-planes for the subsonic model, which had no wakes off the nozzles. The streamlines generated by the program verified that the flow was well-behaved, with no drastic changes in flow direction as the flow passed by the exit-planes.

PAN AIR predictions for the baseline canard/wing configuration as well as a canard-off configuration were compared with results from the Ames 11- by 11-Foot Transonic Wind Tunnel. Results were compared at Mach numbers of 0.6, 0.9, and 1.2, and at angles of attack from 0° to 10°. These comparisons showed that PAN AIR was capable of predicting subsonic and supersonic results for a complex aircraft geometry which were generally in good agreement with experimental data.

## ACKNOWLEDGEMENT

The authors wish to thank Paul Keller of Informatics General Corporation for his invaluable assistance with the formation of the PAN AIR definition of the 279 model.

## REFERENCES


1. Towne, M. C.; Strande, S. M.; Erickson, L. L.; Kroo, I. M.; Enomoto, F. Y., Carmichael, R. L.; and McPherson, K. F.: PAN AIR Modeling Studies. AIAA Paper 83-1830, 1983.

2. Strande, S. M.; Erickson, L. L.; Snyder, L. D.; and Carmichael, R. L.: PAN AIR Modeling Studies II: Side Slip Option, Network Gaps, Three Dimensional Forebody Flow and Thick Trailing Edge Representation. AIAA Paper 84-0220, 1984.

3. Carmichael, R. L.; and Erickson, L. L.: PAN AIR--A Higher Order Panel Method for Predicting Subsonic or Supersonic Linear Potential Flows About Arbitrary Configurations. AIAA Paper 81-1255, 1981.

4. Miller, S. G.; and Youngblood, D. B.: Applications of USSAERO-B and the PANAIR Production Code to the CDAF Model a Canard/Wing Configuration. AIAA Paper 83-1829, 1983.

5. Magnus, A. E.; and Epton, M. A.: PAN AIR--A Computer Program for Predicting Subsonic or Supersonic Linear Potential Flows About Arbitrary Configurations Using a Higher Order Panel Method, Vol. I, Theory Document (Version 1.1). NASA CR-3251, 1981.

6. Sidwell, K. W.; Baruah, P. K.; and Bussoletti, J. E.: PAN AIR--A Computer Program for Predicting Subsonic or Supersonic Linear Potential Flows About Arbitrary Configurations Using a Higher Order Panel Method, Vol. II, User Manual (Version 1.1). NASA CR-3252, 1981.

7. Sidwell, K. W., ed.: PAN AIR--A Computer Program for Predicting Subsonic or Supersonic Linear Potential Flows About Arbitrary Configurations Using a Higher Order Panel Method, Vol. III, Case Manual (Version 1.1). NASA CR-3253, 1981.

8. Baruah, P. K.; Bussoletti, J. E.; Massena, W. A.; Nelson, F. D.; Purdon, D. J.; and Tsurusaki, K.: PAN AIR--A Computer Program for Predicting Subsonic or Supersonic Linear Potential Flows About Arbitrary Configurations Using a Higher Order Panel Method, Vol. IV, Maintenance Document (Version 1.1). NASA CR-3251, 1981.

9. Johnson, F. T.; and Tinoco, E. N.: Recent Advances in the Solution of Three-Dimensional Flows Over Wings with Leading Edge Vortex Separation. AIAA Paper 79-0282, 1979.

10. Hess, J. R.; and Bear, R. L.: Study of Aerodynamic Technology for Single-Cruise-Engine V/STOL Fighter/Attack Aircraft, Phase I Final Report. NASA CR-166269, 1982.

TABLE 1.- NOZZLE EXIT MODELS

| MODEL | NOZZLE EXIT PLANES* | NOZZLE WAKES | | |
|---|---|---|---|---|
| 1 | NO | NO | | SUPERSONIC |
| 2 | NO | YES | | |
| 3 | YES | NO | SUBSONIC | |
| 4 | YES | YES | | |

*BASE NETWORKS

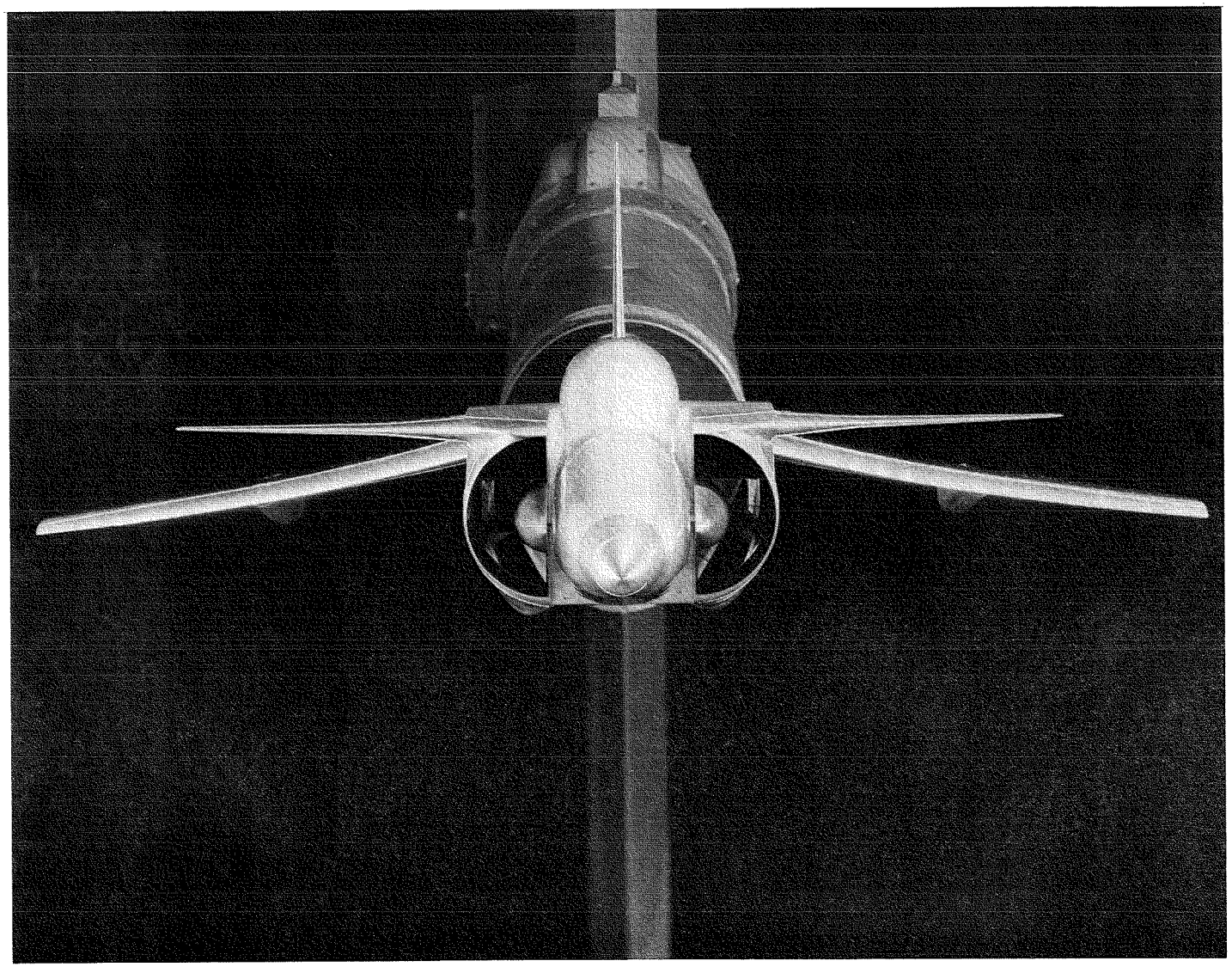

(a) Front view.

Figure 1.- Wind tunnel force model installed in Ames 11- by 11-Foot Transonic Wind Tunnel.

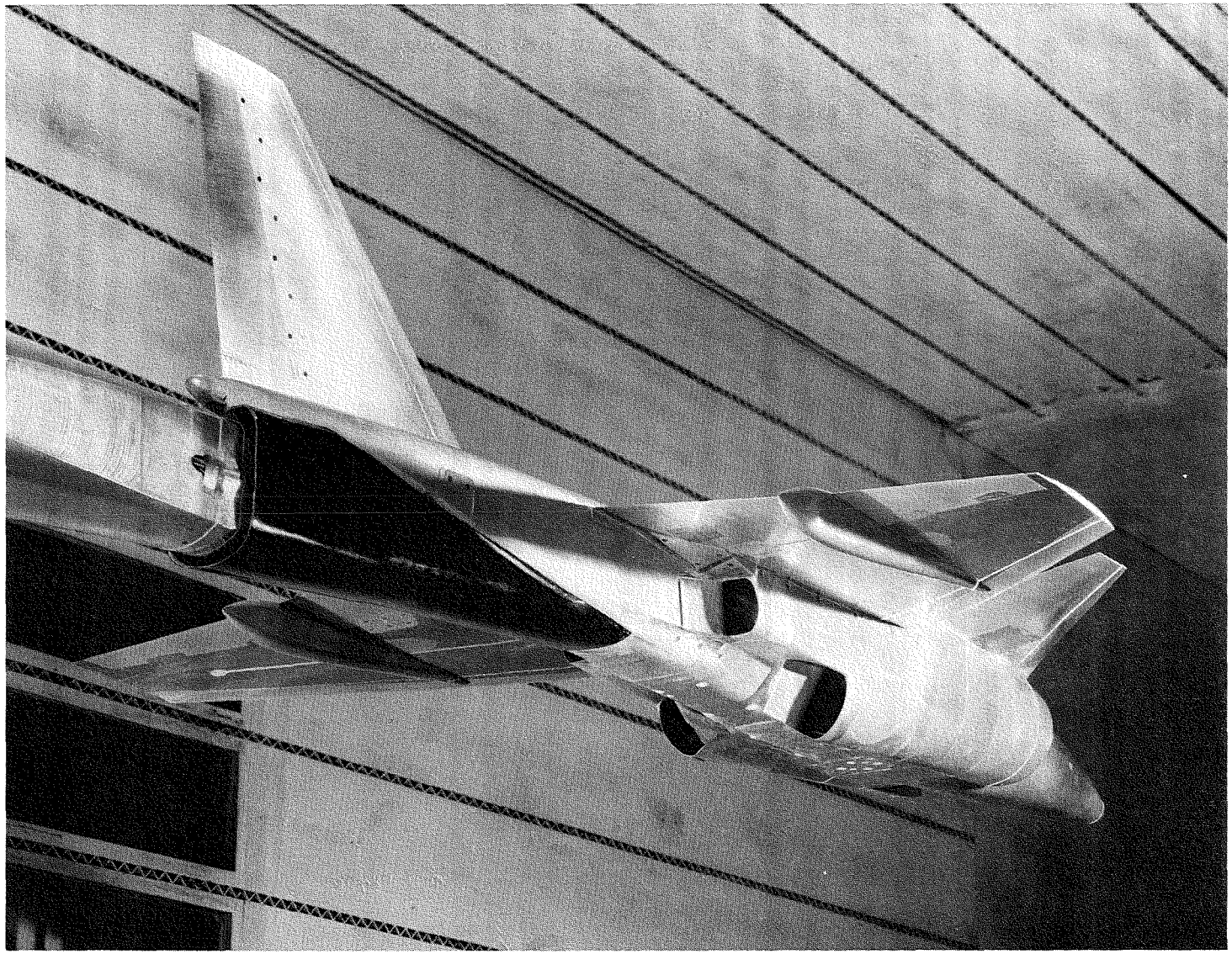

(b) Bottom view.

Figure 1.- Continued.

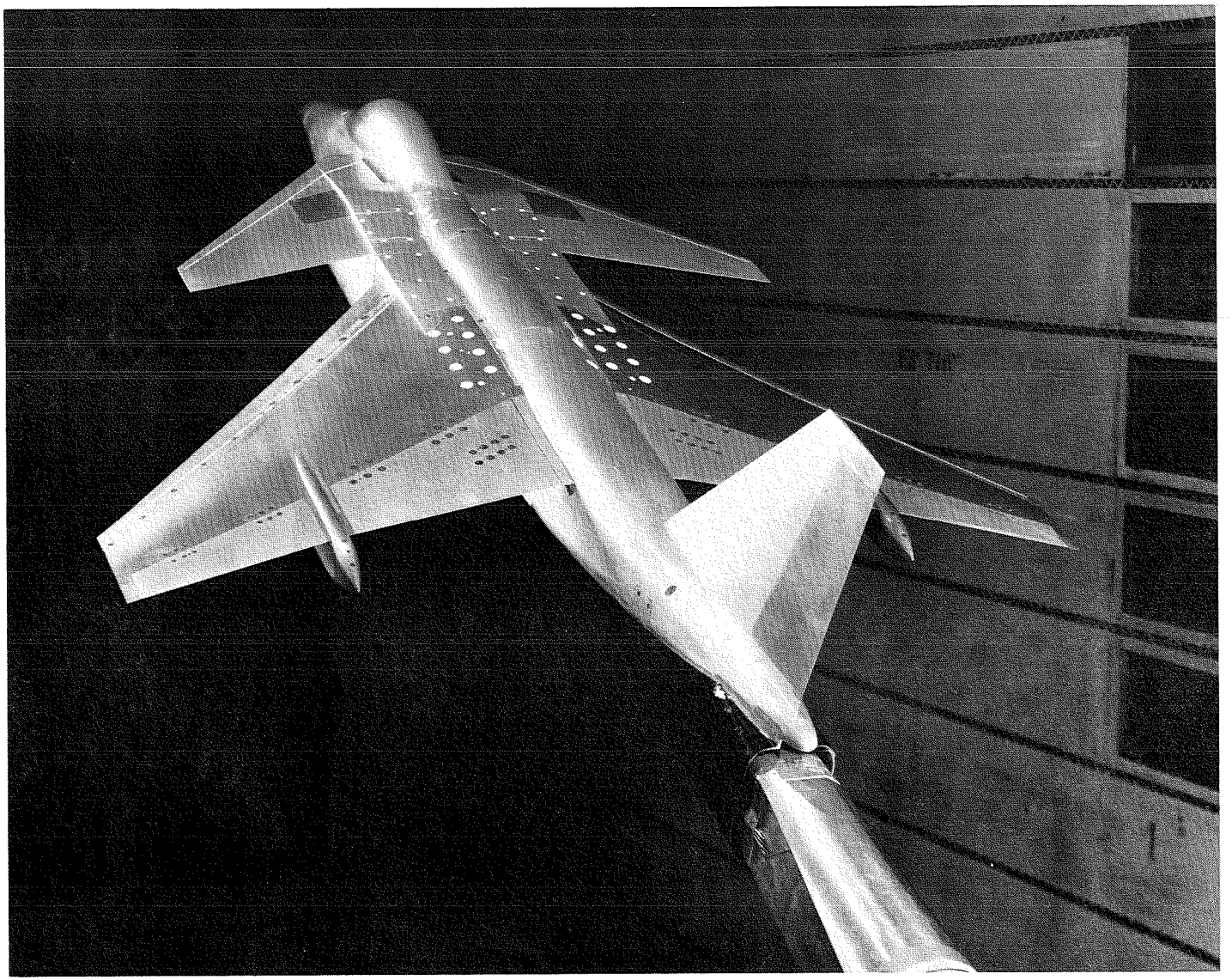

(c) Top view.

Figure 1.- Concluded.

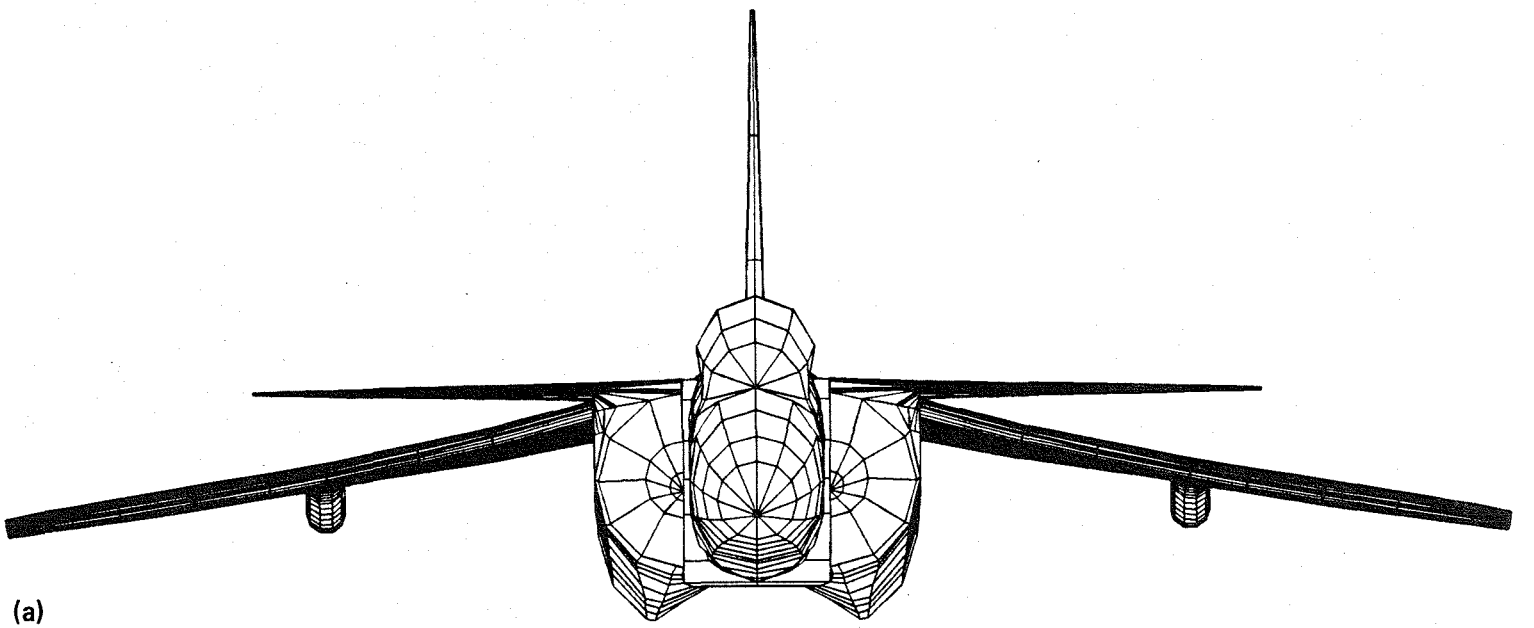


(a) Front view.

Figure 2.- PAN AIR paneling of the baseline (canard-on) configuration.

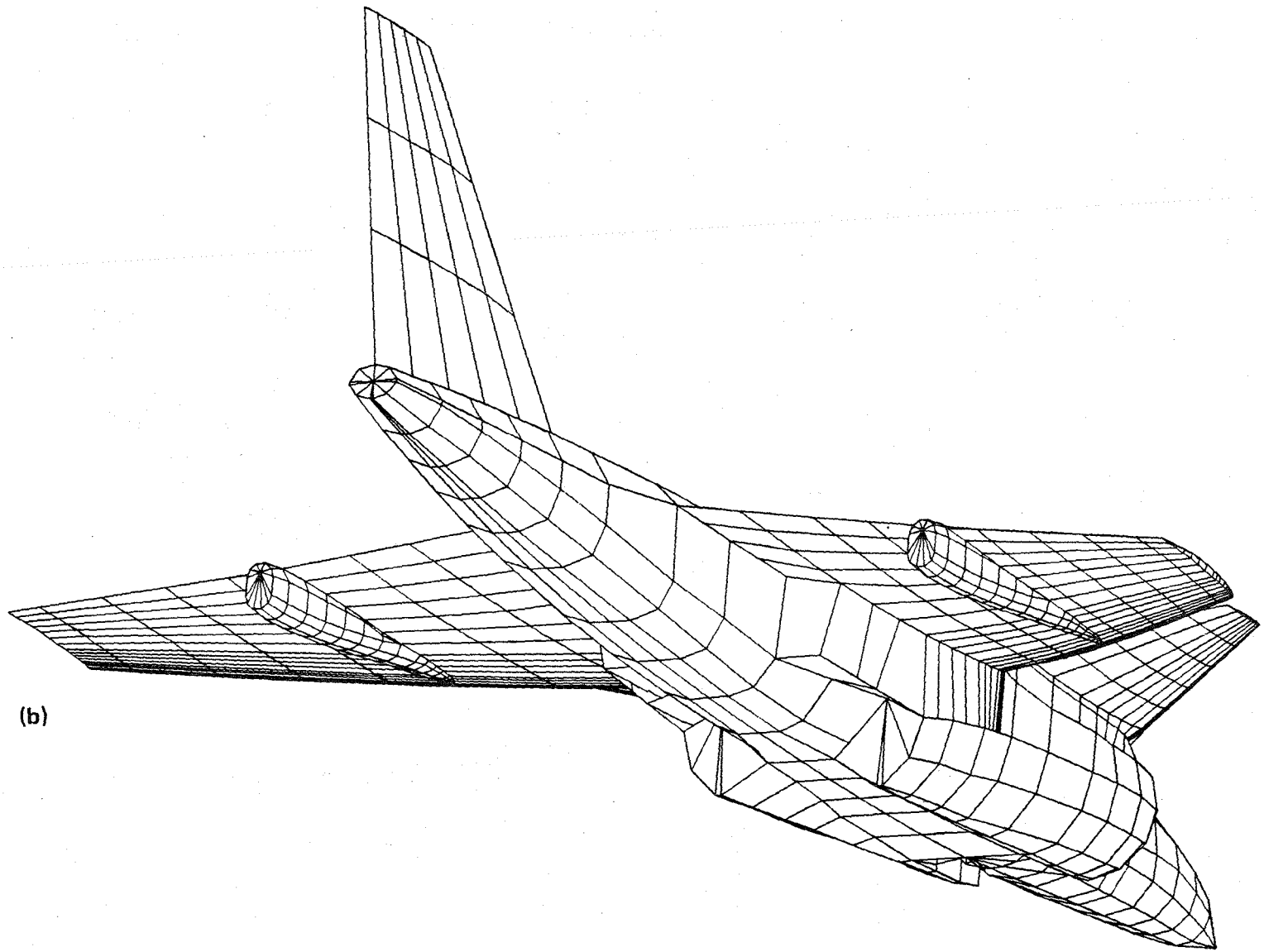


(b) Bottom view.

Figure 2.- Continued.

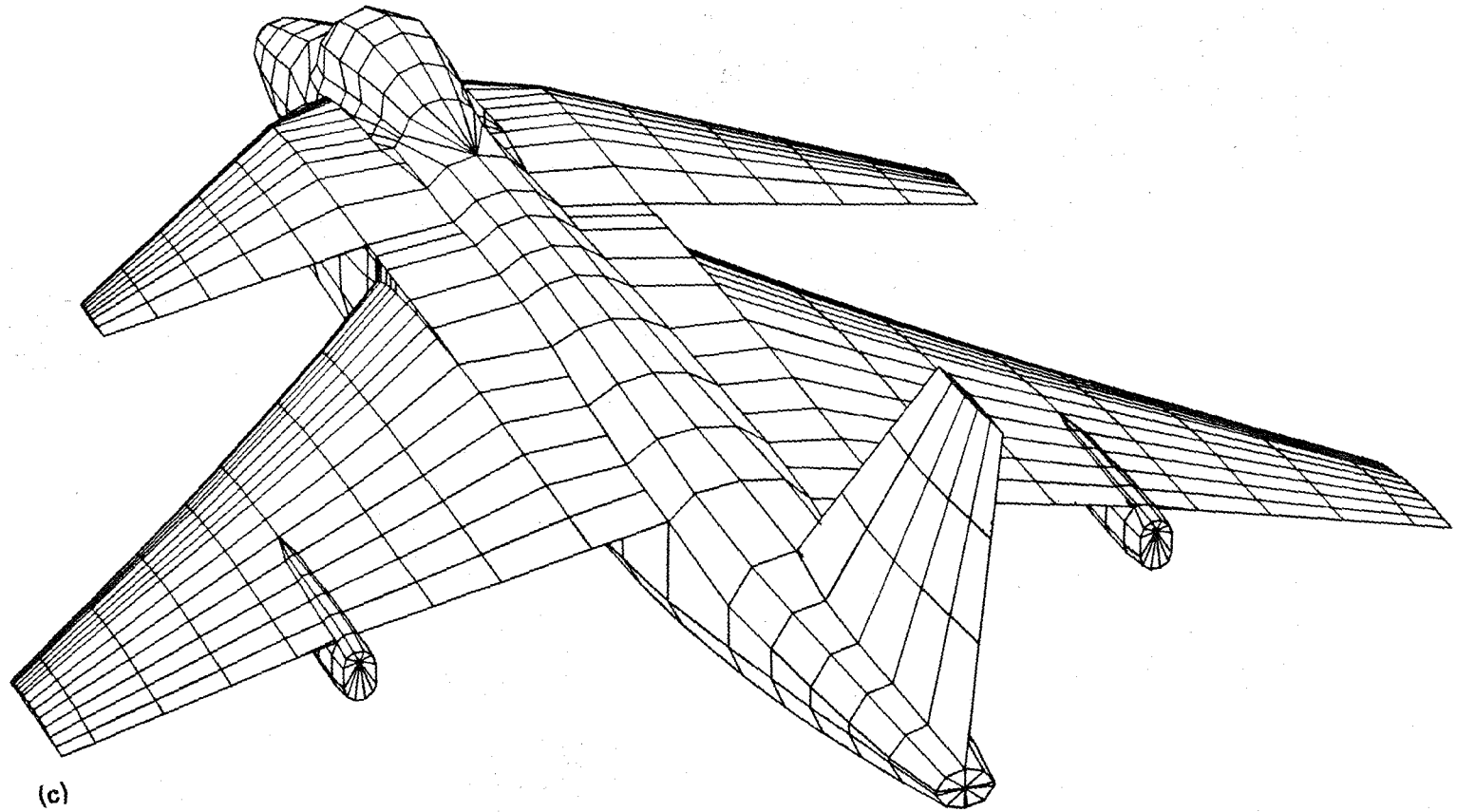


(c) Top view.

Figure 2.- Concluded.

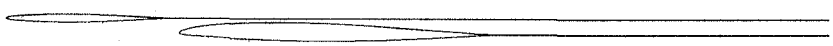

Figure 3.- Canard and wing root sections with wakes defined in the chord plane.

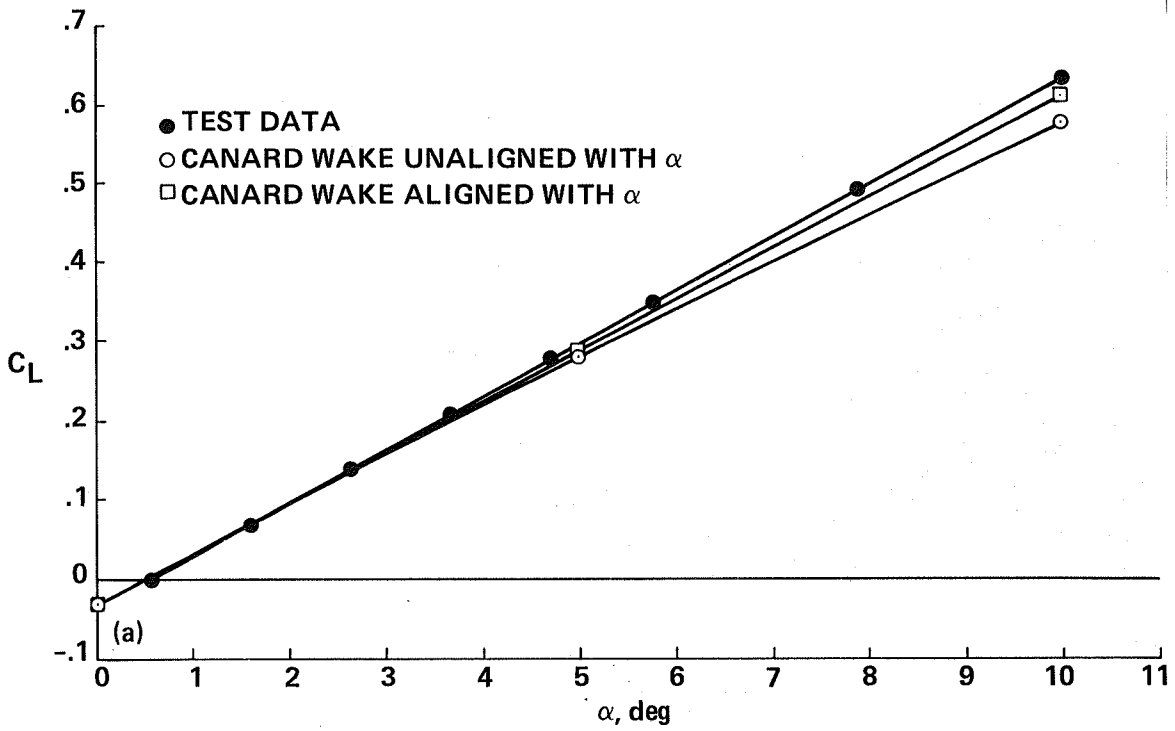


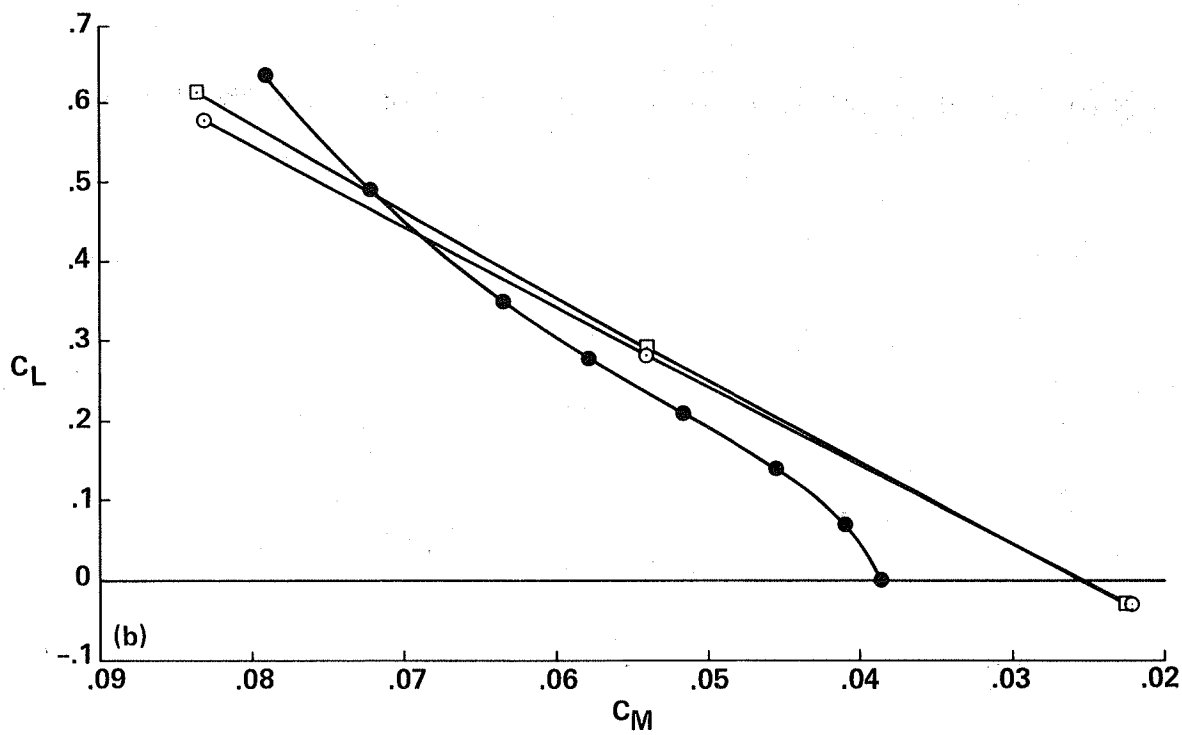


(a) Lift.

(b) Pitching moment.

Figure 4.- Effect of canard wake location on PAN AIR results, $M_\infty$ = 0.6.

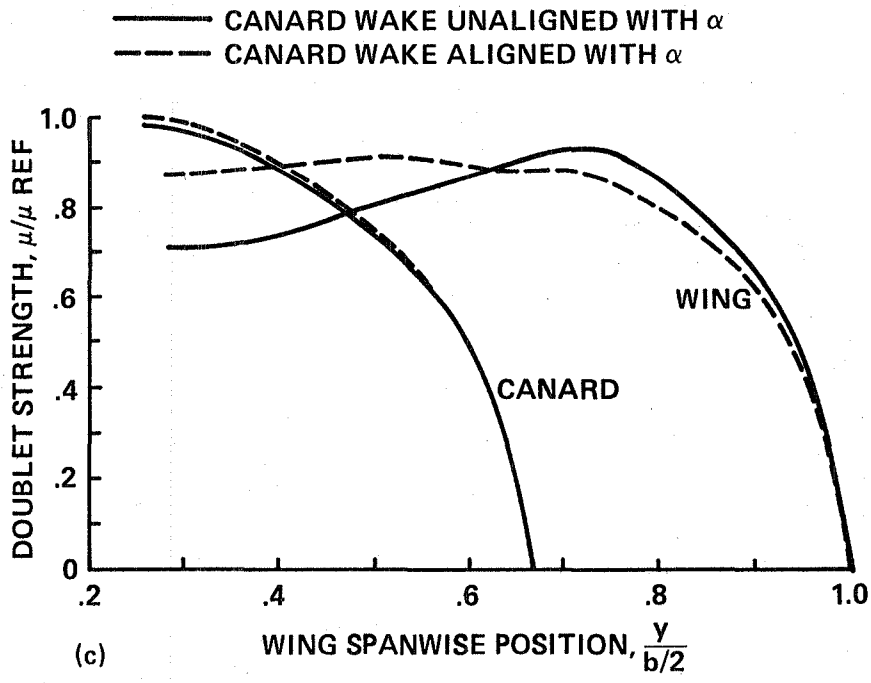


(c) Doublet distribution, $\alpha = 10°$.

Figure 4.- Concluded.

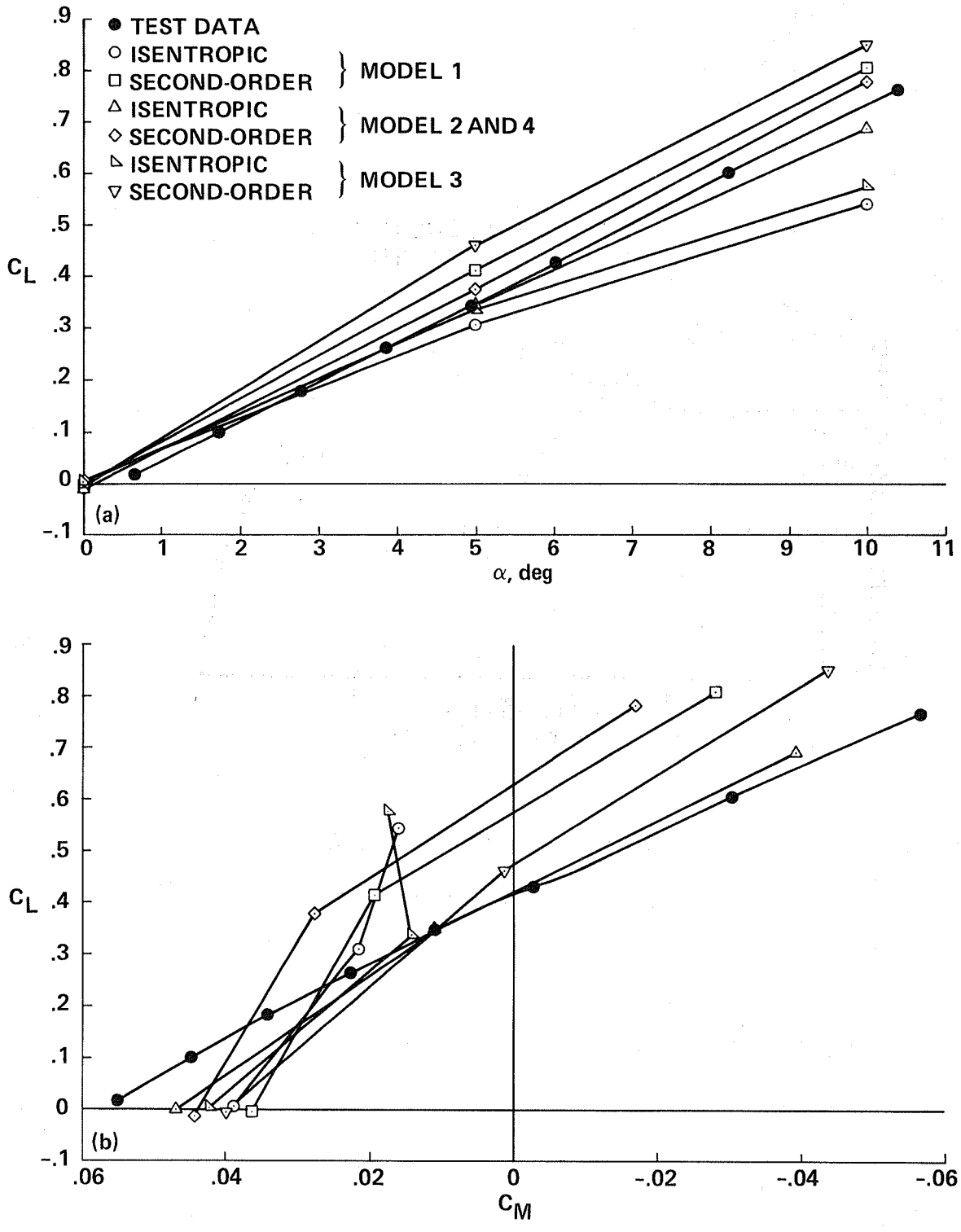


Figure 5.- PAN AIR results for supersonic nozzle exit models, $M_\infty$ = 1.2. (a) Lift; (b) pitching moment.

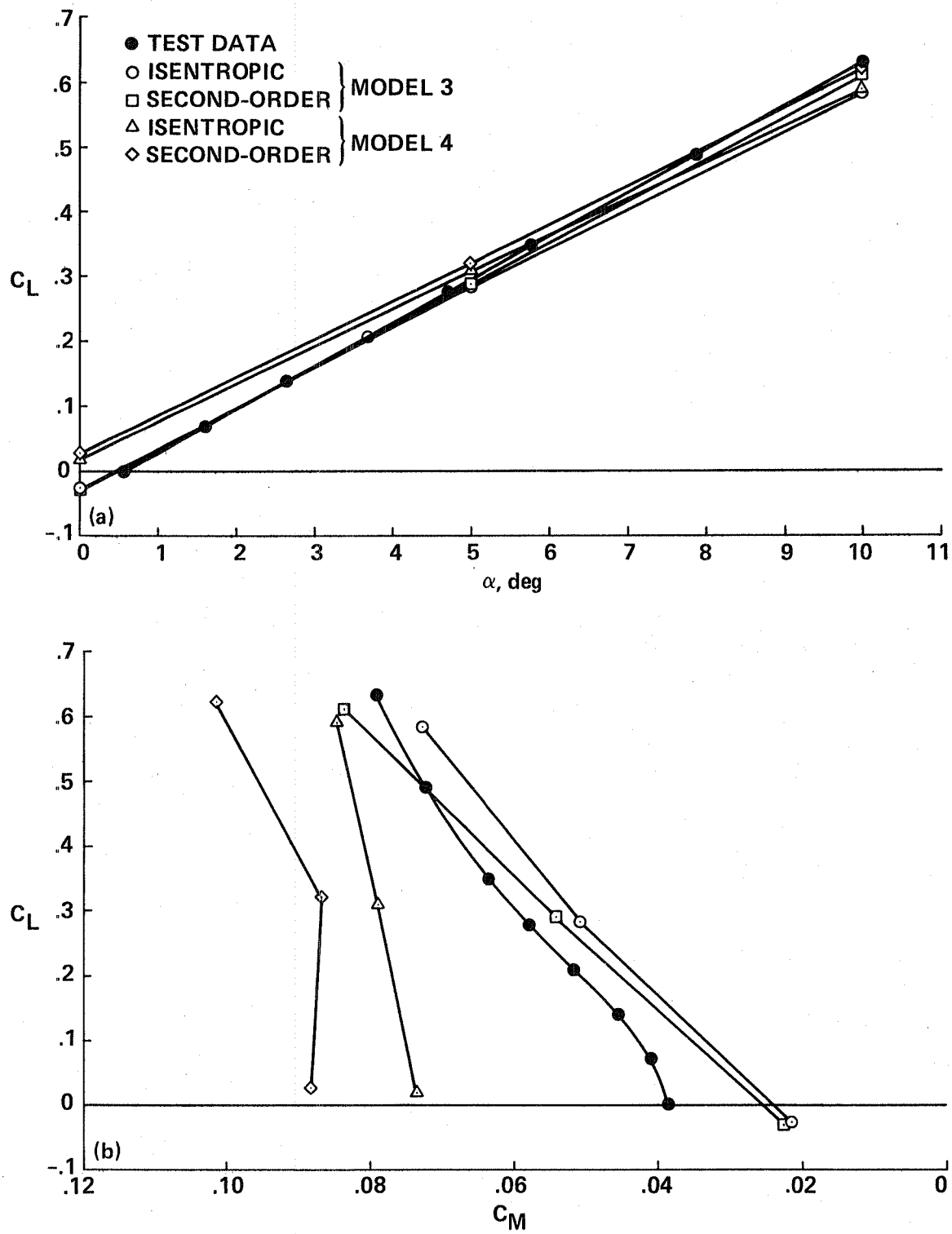


Figure 6.- PAN AIR results for subsonic nozzle exit models, $M_\infty$ = 0.6. (a) Lift; (b) pitching moment.

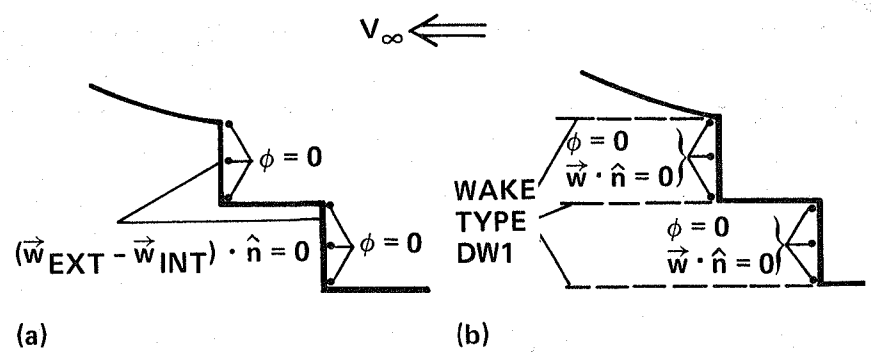


Figure 7.- Nozzle exit plane models used to obtain final PAN AIR data for comparison with wind tunnel results. (a) Subsonic; (b) supersonic.

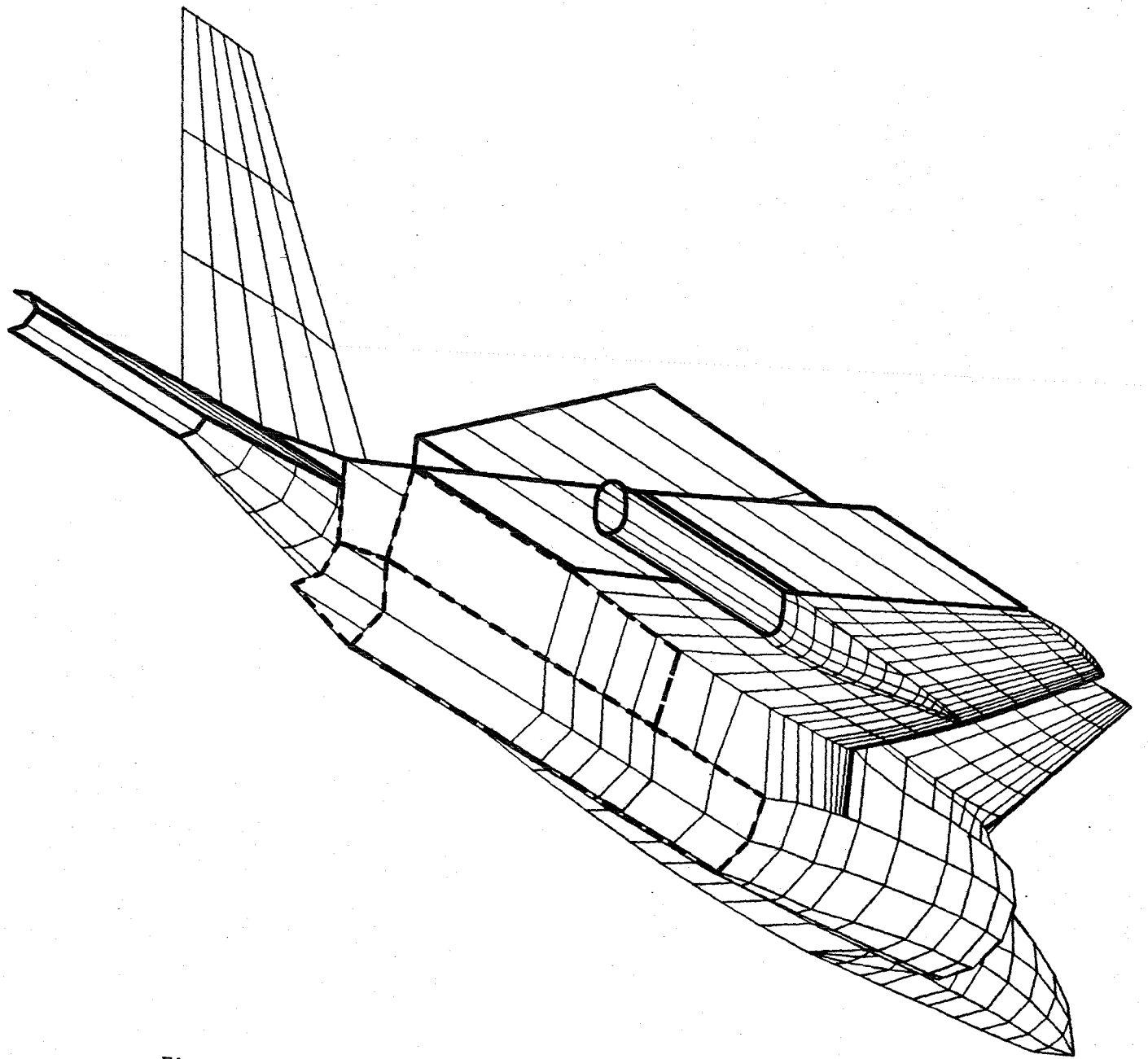

Figure 8.- Location of nozzle wakes for supersonic PAN AIR model (Model 4).

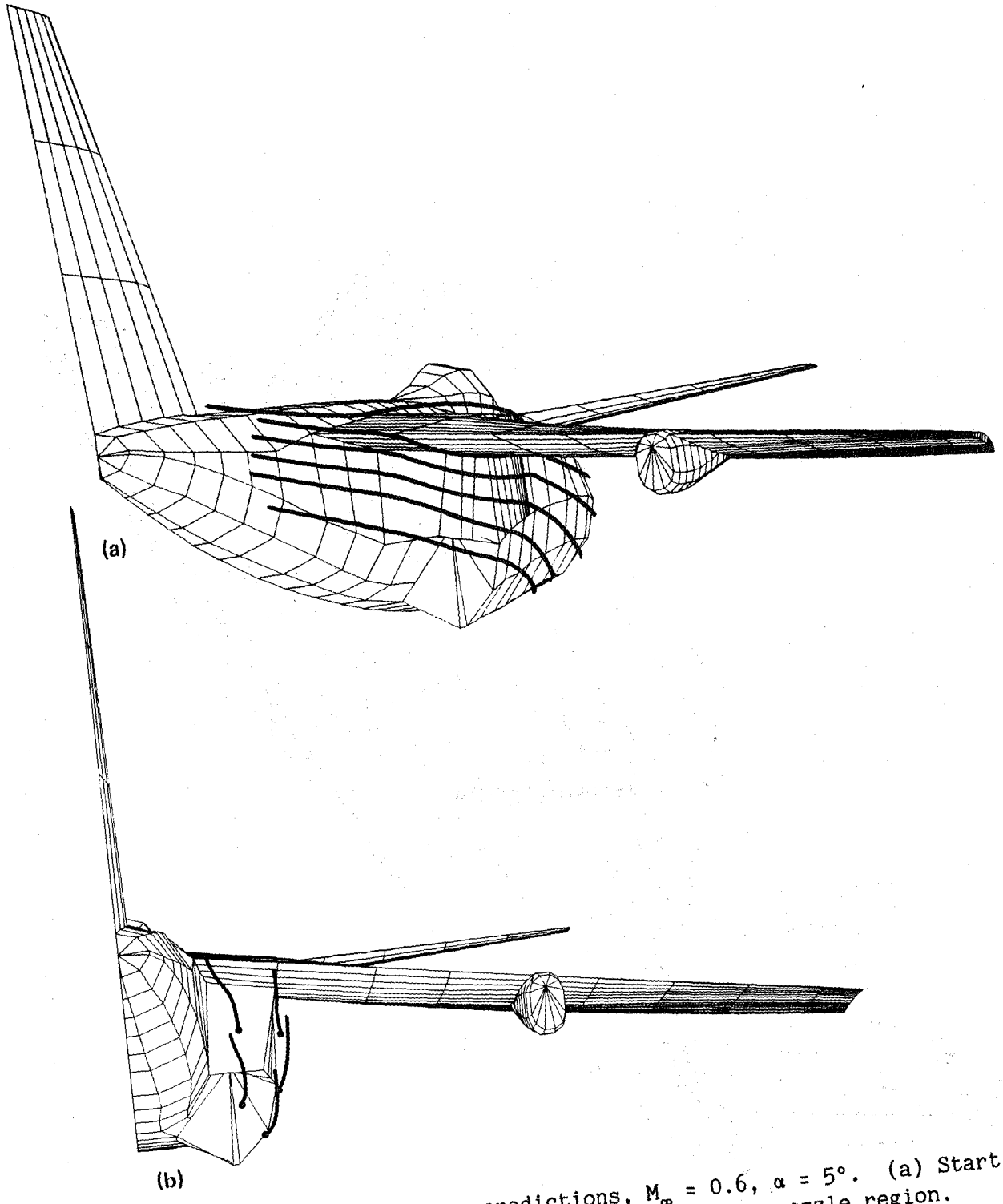


Figure 9.- PAN AIR streamline predictions, $M_\infty = 0.6$, $\alpha = 5°$. (a) Starting from nacelle leading edge; (b) starting from nozzle region.

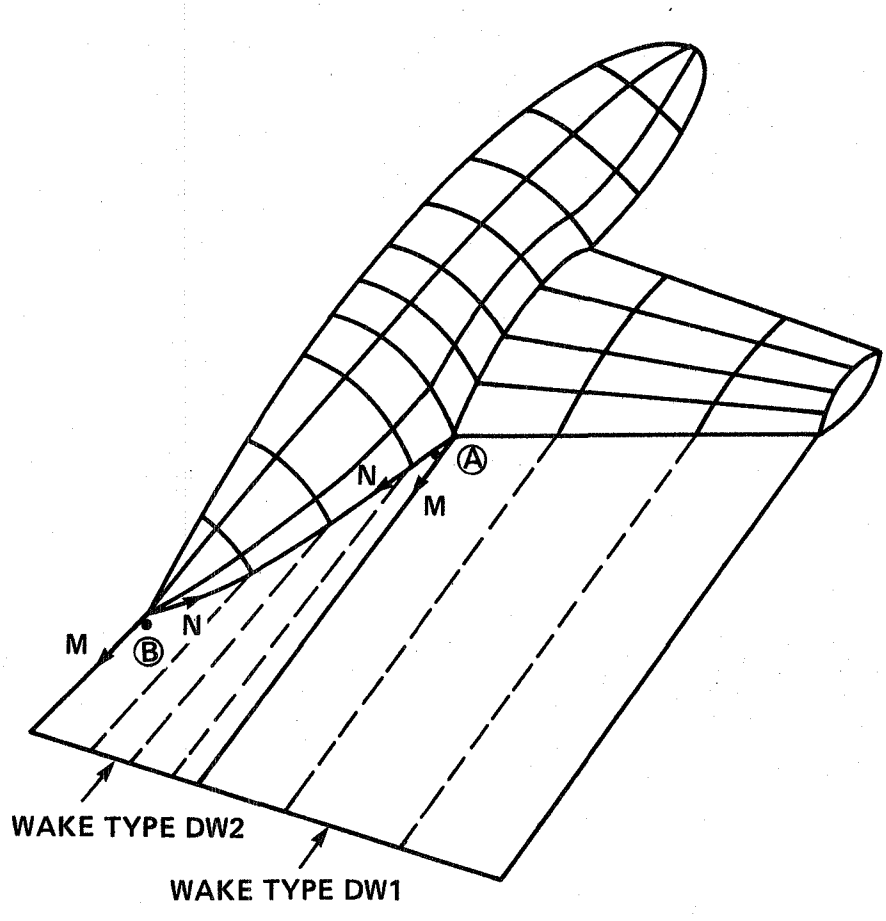


Figure 10.- Correct (Pt. A) and incorrect (Pt. B) origin location for a PAN AIR constant strength doublet wake network (Type DW2).

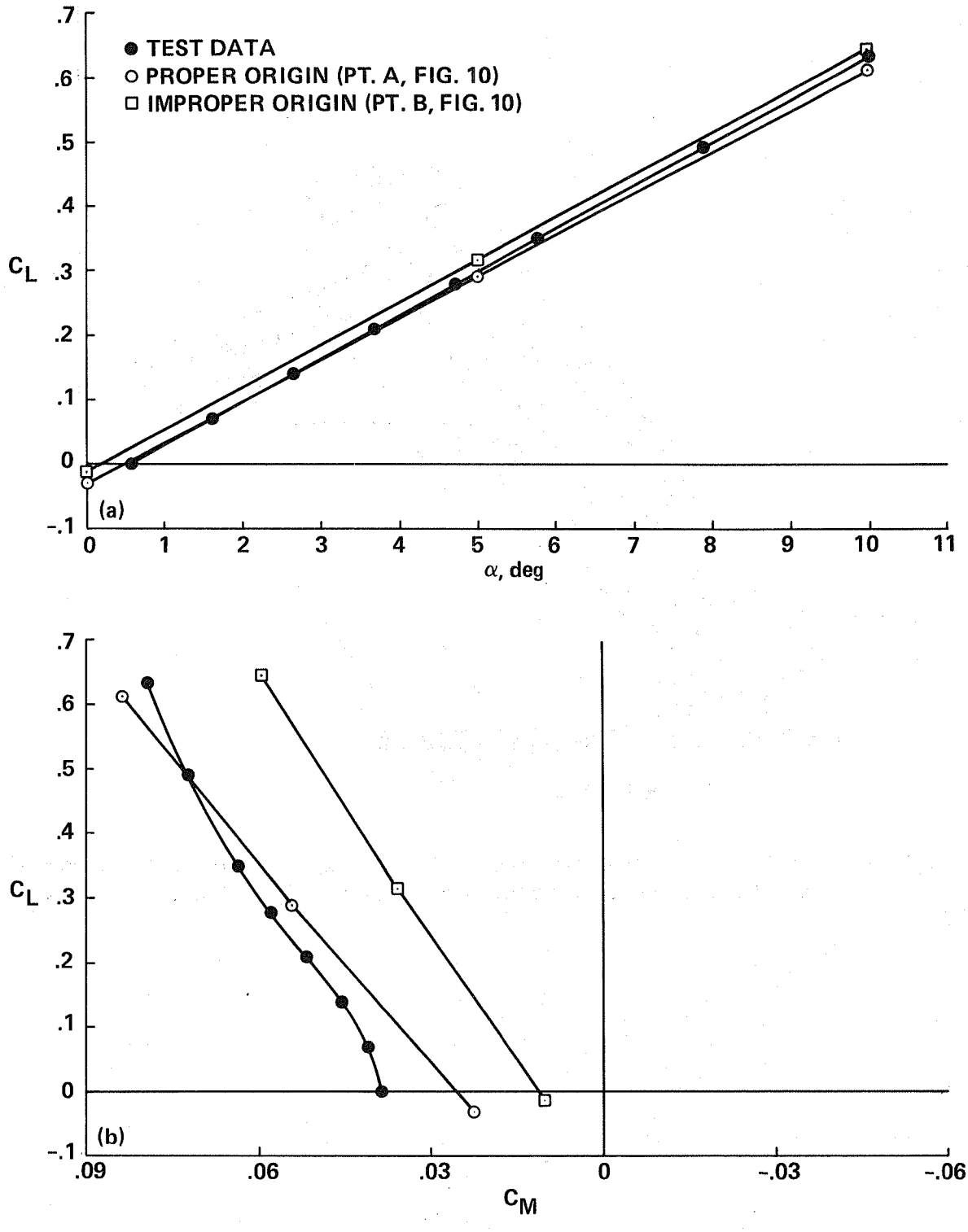


Figure 11.- Effect of wake type DW2 origin location on PAN AIR results. (a) Lift; (b) pitching moment.

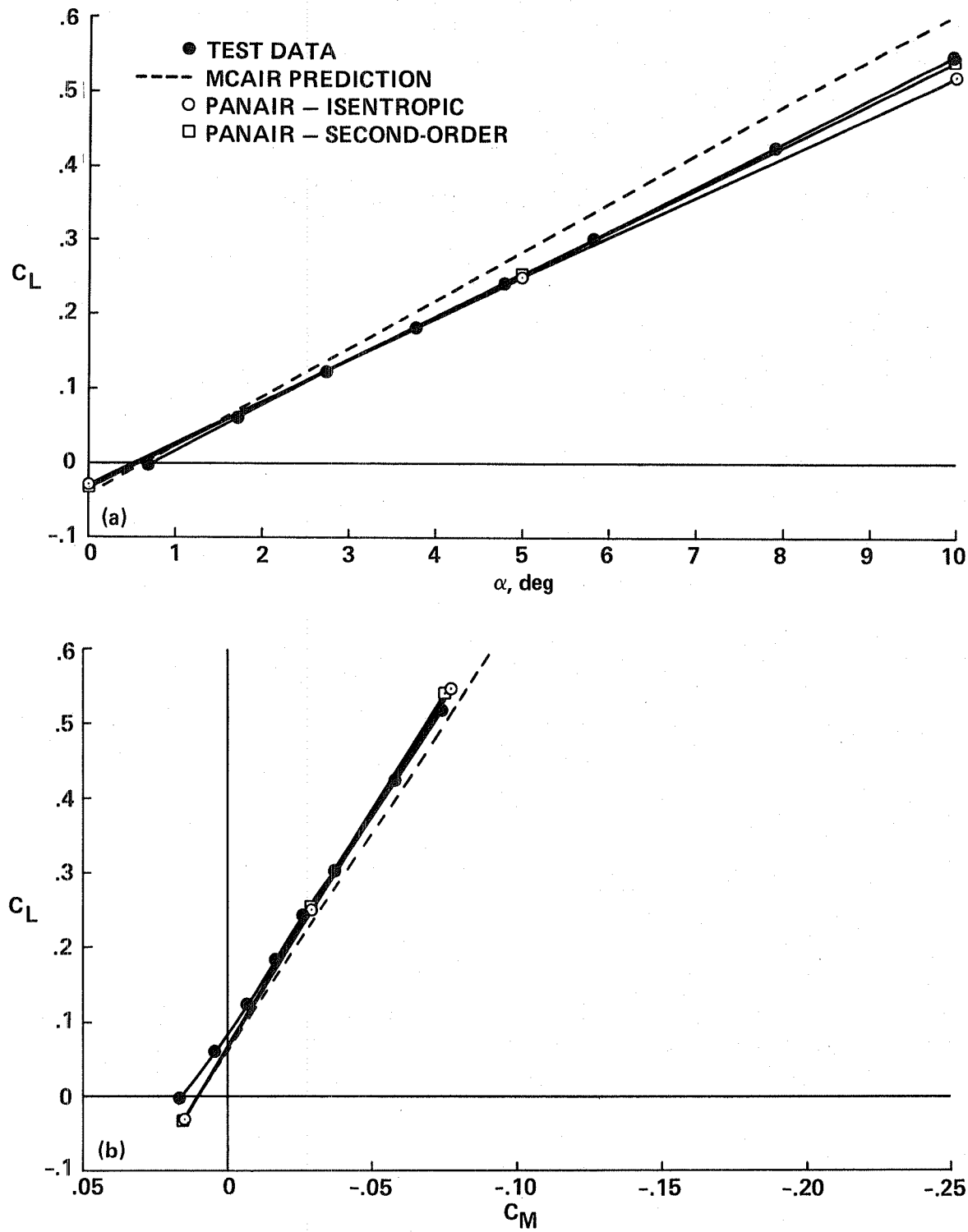


Figure 12.- Comparison of PAN AIR results with wind tunnel test data; canard-off configuration, $M_\infty = 0.6$. (a) Lift; (b) pitching moment.

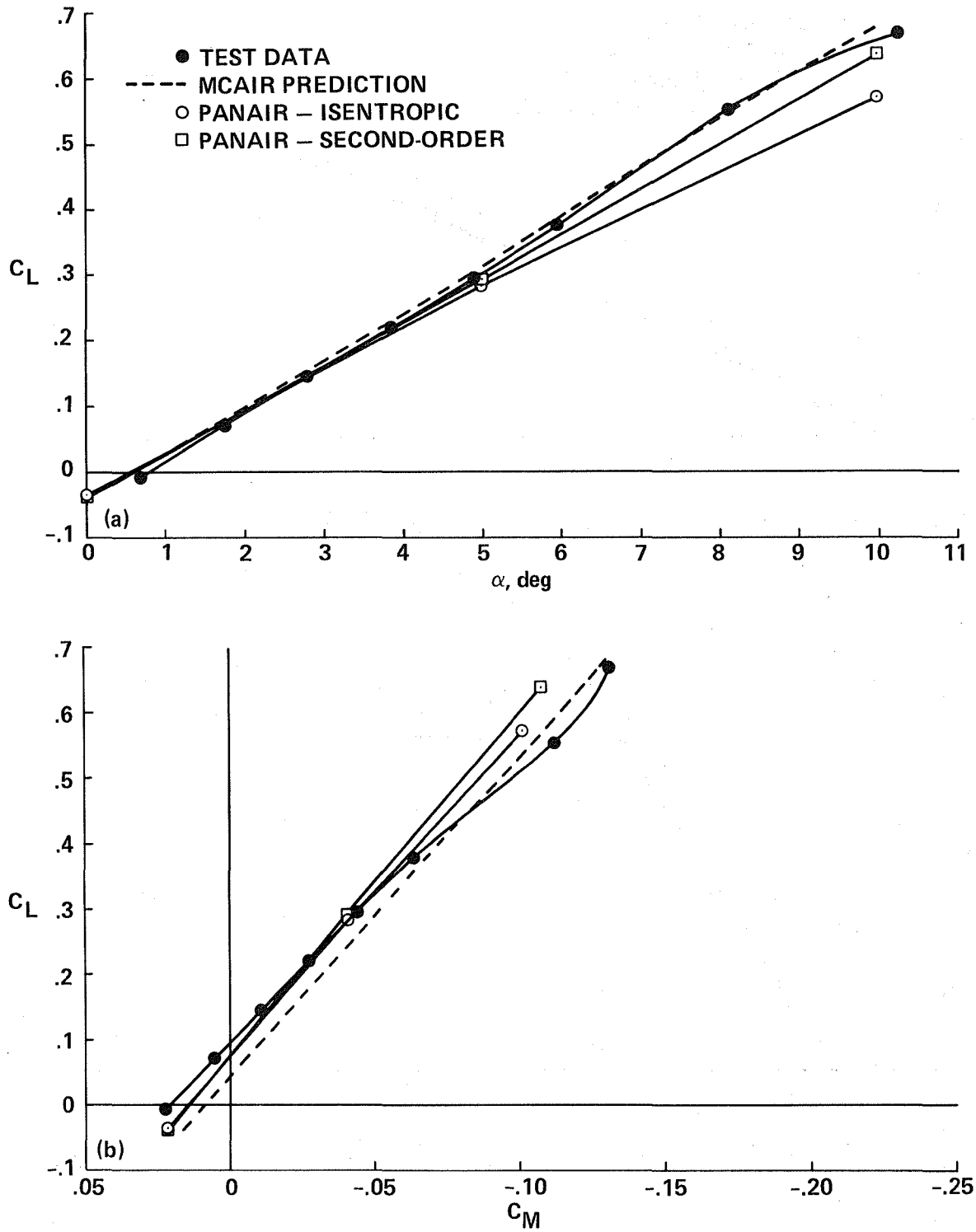


Figure 13.- Comparison of PAN AIR results with wind tunnel test data; canard-off configuration, $M_\infty$ = 0.9. (a) Lift; (b) pitching moment.

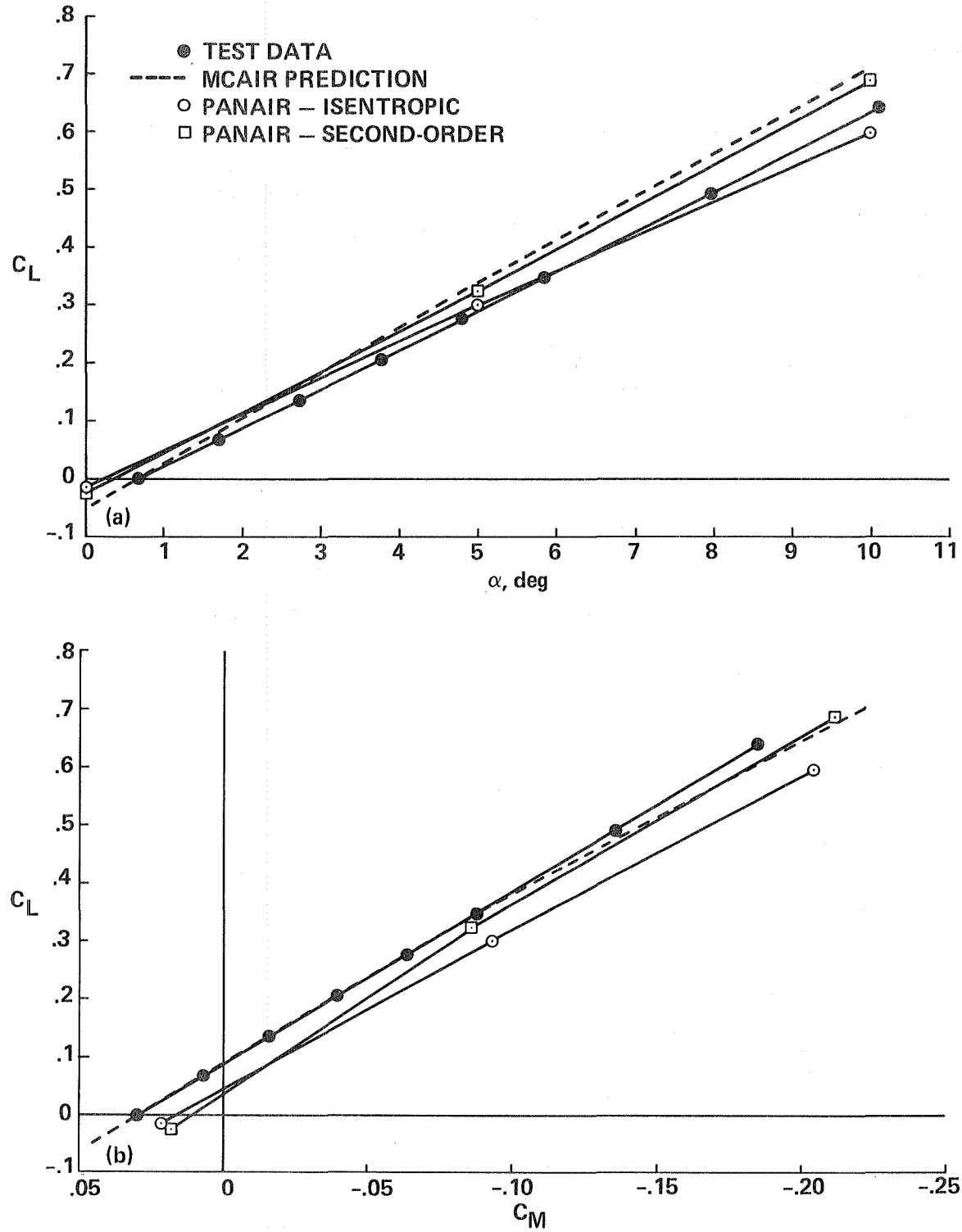


Figure 14.- Comparison of PAN AIR results with wind tunnel test data; canard-off configuration, $M_\infty$ = 1.2. (a) Lift; (b) pitching moment.

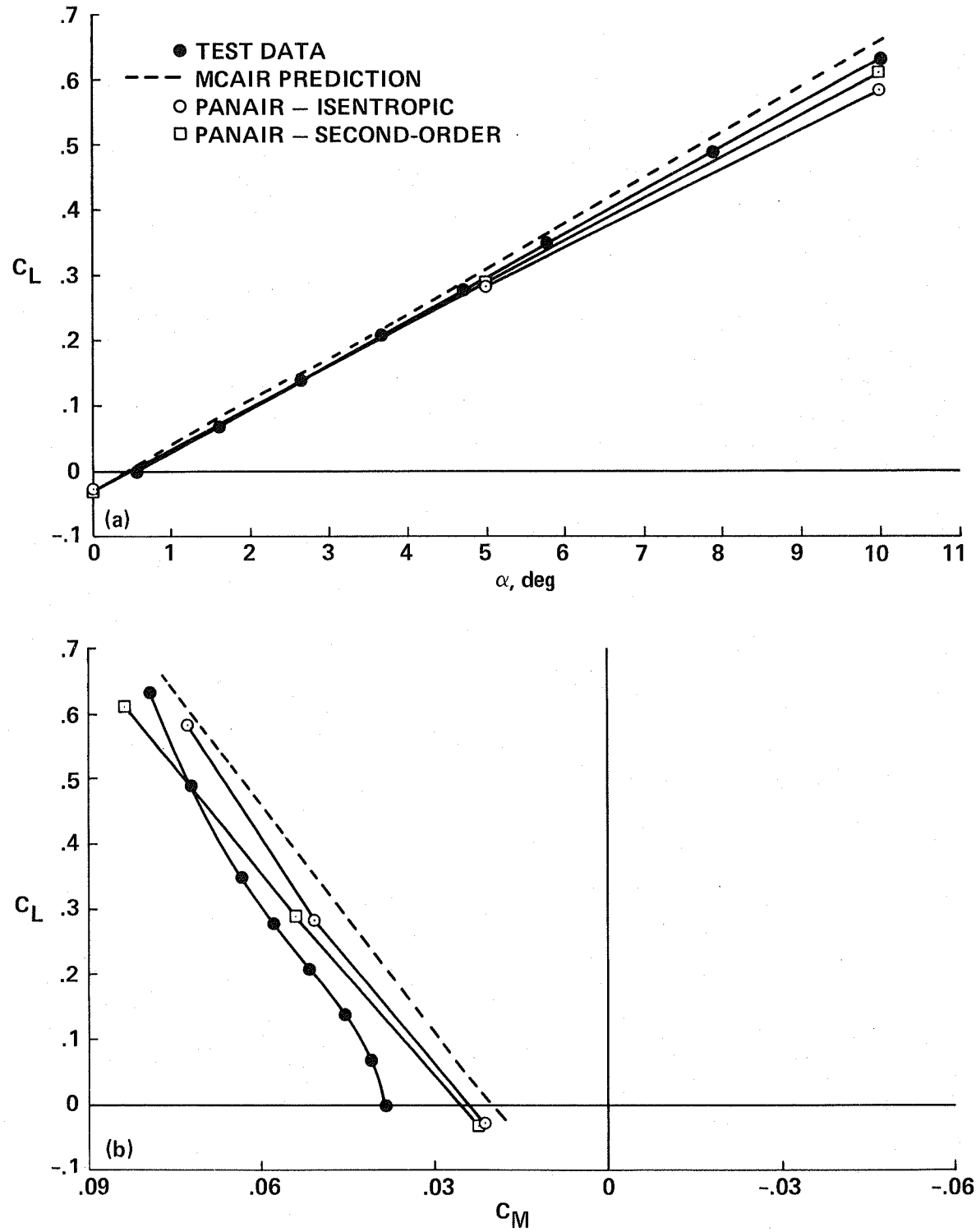


Figure 15.- Comparison of PAN AIR results with wind tunnel test data; baseline (canard-on) configuration, $M_\infty$ = 0.6. (a) Lift; (b) pitching moment.

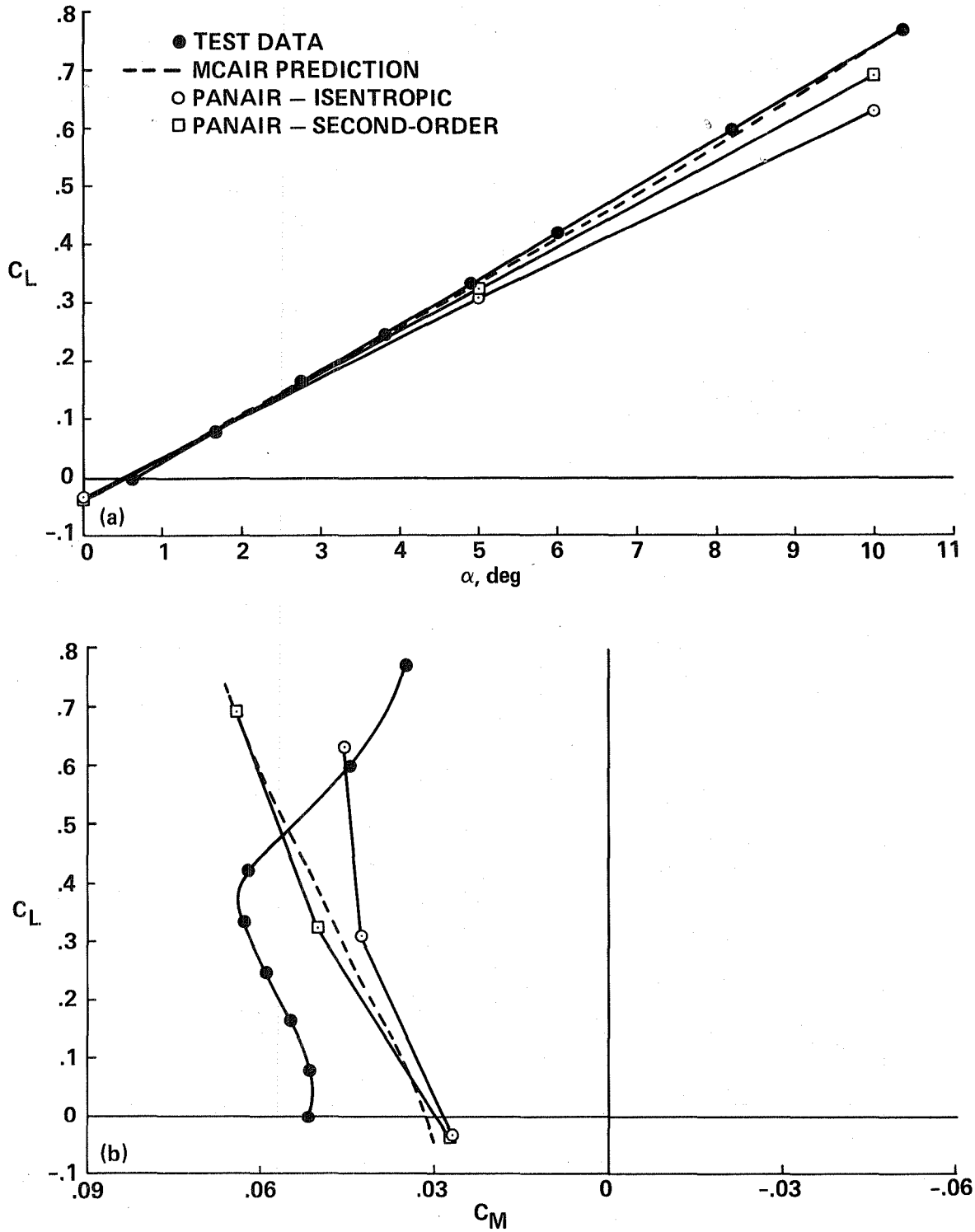


Figure. 16.- Comparison of PAN AIR results with wind tunnel test data; baseline (canard-on) configuration, $M_\infty = 0.9$. (a) Lift; (b) pitching moment.

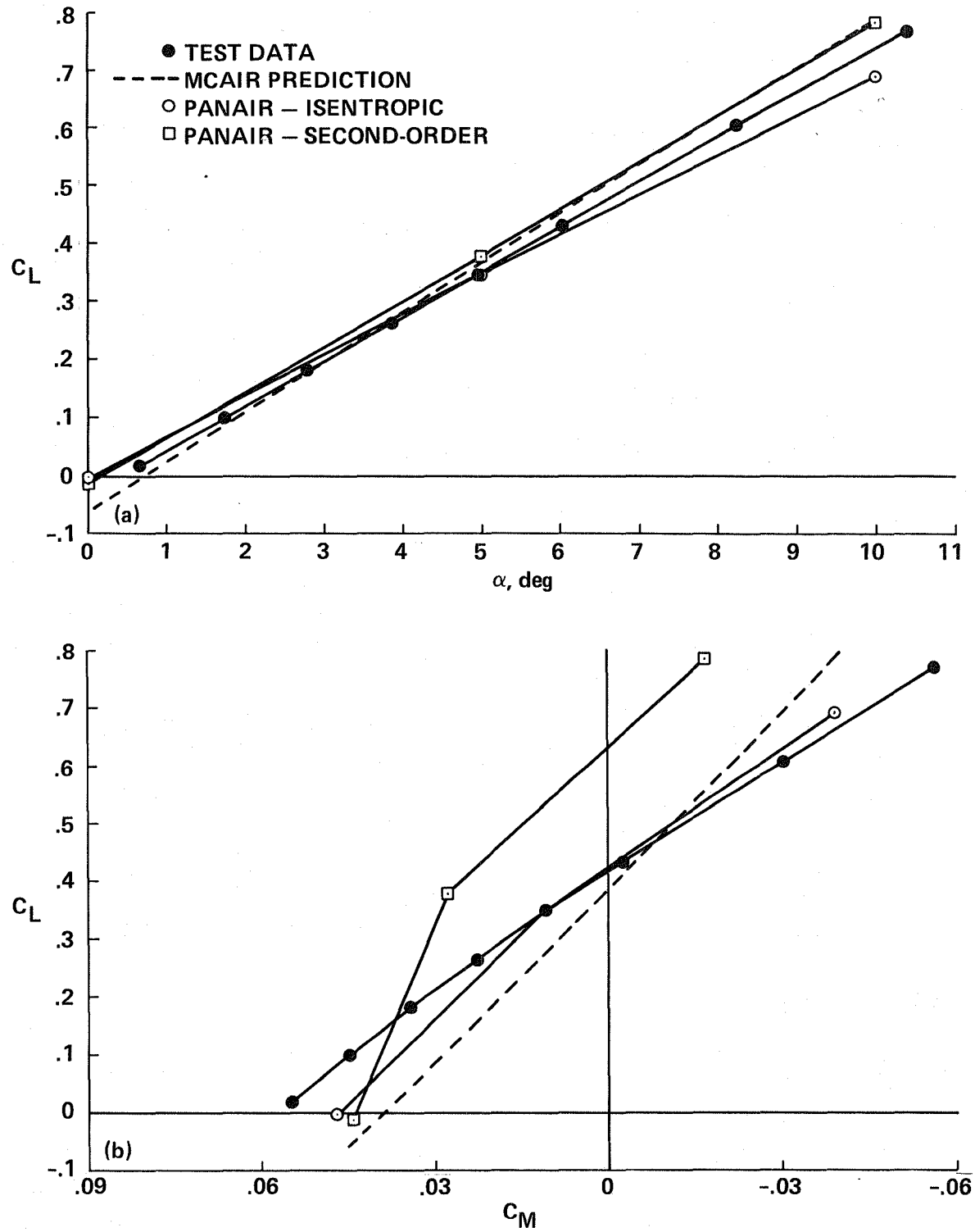


Figure 17.- Comparison of PAN AIR results with wind tunnel test data; baseline (canard-on) configuration, $M_\infty$ = 1.2. (a) Lift; (b) pitching moment.

| 1. Report No. | 2. Government Accession No. | 3. Recipient's Catalog No. |
|---|---|---|
| NASA TM-86838 | | |

| 4. Title and Subtitle | 5. Report Date |
|---|---|
| PAN AIR ANALYSIS OF THE NASA/MCAIR 279-3: AN ADVANCED SUPERSONIC V/STOL FIGHTER/ATTACK AIRCRAFT | April 1986 |
| | 6. Performing Organization Code |
| 7. Author(s) | 8. Performing Organization Report No. |
| Michael D. Madson and Larry L. Erickson | A-85414 |
| | 10. Work Unit No. |
| 9. Performing Organization Name and Address | |
| Ames Research Center<br>Moffett Field, CA 94035 | 11. Contract or Grant No. |
| | 13. Type of Report and Period Covered |
| 12. Sponsoring Agency Name and Address | Technical Memorandum |
| National Aeronautics and Space Administration<br>Washington, DC 20546 | 14. Sponsoring Agency Code |
| | 505-31-21 |

15. Supplementary Notes

Point of contact: Michael D. Madson, Ames Research Center, M/S 227-2, Moffett Field, CA 94035 (415) 694-6010 or FTS 464-6010

16. Abstract

PAN AIR is a computer program for predicting subsonic or supersonic linear potential flow about arbitrary configurations. The program was applied to a highly complex single-engine-cruise V/STOL fighter/attack aircraft. Complexities include a close-coupled canard/wing, large inlets, and four exhaust nozzles mounted directly under the wing and against the fuselage. Modeling uncertainties involving canard wake location and flow-through approximation through the inlet and the exhaust nozzles were investigated. The recently added streamline capability of the program was utilized to evaluate visually the predicted flow over the model. PAN AIR results for Mach numbers of 0.6, 0.9, and 1.2 at angles of attack of 0, 5, and 10° were compared with data obtained in the Ames 11- by 11-Foot Transonic Wind Tunnel, at a Reynolds number of $3.69 \times 10^6$ based on $\bar{c}$.

| 17. Key Words (Suggested by Author(s)) | 18. Distribution Statement |
|---|---|
| PAN AIR<br>V/STOL<br>Supersonic | ~~Limited~~<br>Subject category - 02 |

| 19. Security Classif. (of this report) | 20. Security Classif. (of this page) | 21. No. of Pages | 22. Price* |
|---|---|---|---|
| Unclassified | Unclassified | 39 | |

*For sale by the National Technical Information Service, Springfield, Virginia 22161

End of Document